Dapsone Form V: A Late Appearing Thermodynamic Polymorph of a Pharmaceutical

Doris E. Braun,[†,] Martin Vickers[‡] and Ulrich J. Griesser[†]*

[†]Institute of Pharmacy, University of Innsbruck, Innrain 52c, 6020 Innsbruck, Austria

[‡]Department of Chemistry, University College London, 20 Gordon Street, London WC1H 0AJ, U.K.

KEYWORDS: dapsone, polymorph, kinetic and thermodynamic stability, transformation, X-ray diffraction, thermal analysis, solution calorimetry, crystal structure prediction, lattice energy

Abstract

Five anhydrate polymorphs (Forms **I** – **V**) and the isomorphic dehydrate (**Hy$_{dehy}$**) of dapsone (*4,4′*-diaminodiphenyl sulfone or DDS) were prepared and characterized in an interdisciplinary experimental and computational study, elucidating the kinetic and thermodynamic stabilities, solid form interrelationships and structural features of the known forms **I** – **IV**, the novel polymorph **Form V**, and **Hy$_{dehy}$**. Calorimetric measurements, solubility experiments and lattice energy calculations revealed that **Form V** is the thermodynamically stable polymorph from absolute zero to at least 90 °C. At higher temperatures **Form II** and then **Form I** becomes the most stable DDS solid form. The computed 0 K stability order (lattice energy calculations) was confirmed with calorimetric measurements as follows: **V** (most stable) > **III** > **Hy$_{dehy}$** > **II** > **I** > **IV** (least stable). The discovery of **Form V** was complicated by the fact that the metastable but kinetically stabilized **Form III** shows a higher nucleation and growth rate. By combining laboratory powder X-ray diffraction data and *ab initio* calculations, the crystal structure of **Form V** ($P2_1/c$, Z′=4) was solved, with a high energy DDS conformation allowing a denser packing and more stable intermolecular interactions, rationalizing the formation of a high Z′ structure. The structures of the **Forms I** and **IV**, only observed from the melt and showing distinct packing features compared to the **Forms II**, **III**, and **V**, were derived from the computed crystal energy landscapes. Dehydration modelling of the DDS hydrate lead to the **Hy$_{dehy}$** structure. This study expands our understanding about the complex crystallization behavior of pharmaceuticals and highlights the big challenge in solid form screening, especially that there is no clear end point.

1. Introduction

The objective of a polymorphism screening is identifying all relevant solid forms, characterizing them, and choosing the optimal form for further chemical and pharmaceutical development. This is an important task in the (pre)formulation phase of drug molecules and the choice of the form is usually a compromise between physical and chemical properties of the API affecting manufacturing processes, stability and aspects of biopharmaceutics.[1] Traditionally, the thermodynamically most stable form is selected for the development of a drug formulation, because it cannot convert into another polymorphic form under normal storage conditions.[2, 3] However, if a compound is capable of forming solvent adducts, exposure to humidity or solvents may induce the transformation to a hydrate or solvate. Hydrates are also very popular components of final dosage forms, as due to the ubiquity of water vapor, a hydrate can be the thermodynamically favored form at ambient conditions. Metastable forms are sometimes deliberately chosen in drug development because of, for instance, a superior solubility behavior, which can result in a significantly better bioavailability compared to the stable form.[2]

Many specific crystallization techniques and strategies applied in screening programs have evolved over time. The basic idea here is to maximise the variables and conditions of crystallization processes. Manual crystallisation methods and automated[4] approaches are both used in polymorph screening. Such classic techniques are often adequate to find numerous solid forms for a broad range of substances, but there are always cases where more specialized and/or tailored approaches are required. The vast number of possible experiments that have led to solid forms, which extends beyond the classical methods,[5-17] makes it hard to create a recipe for complete confidence that all possible solid-state forms are found and impossible to cover the entire crystallization ‘space’. Crystallizing the most stable form can be complicated by the fact that this

form may show a slow nucleation and growth rate, in contrast to metastable form(s), as seen for 4-aminoquinaldine monohydrate Hy1B°.[18] Thus, the elucidation of the sometimes complex solid form landscapes of pharmaceuticals can place a significant burden on the increasingly limited (time) resources dedicated to solid form screening. The biggest problem encountered in experimental solid form screening is the fact that there is no clear end point.[19] The late discovery of more stable forms, as in the case of ritonavir[20] or rotigotine,[21] has taught us about the severe consequences when the solid-state behaviour of a drug molecule is not understood and highlights the fact that finding the most stable crystal form at processing and storing conditions is very important.

Crystal structure prediction (CSP) has been designed to find "the" crystal structure of an organic molecule, starting from the chemical diagram. As the awareness of polymorphism increased, it became apparent that some of the low-energy structures on the computationally generated crystal energy landscapes correspond to experimental polymorphs.[19, 22-24]

In this work, we show how a combination of well-designed experiments and modelling can be used to overcome many hurdles in constructing and understanding the solid form landscape of small organic molecules through the example of dapsone (4,4′-diaminodiphenyl sulfone; DDS, Figure 1). The compound was synthesised for the first time over 100 years ago[25] and about 20 years later (in the 1940s) its microbial activity and therapeutic use for leprosy was first studied. Throughout its history the uses of DDS have expanded to treat a diversity of diseases including leprosy, dermatitis herpetiformis, malaria, and prophylaxis of pneumocytosis.[26, 27] Today, its prime indication is as first-line drug in the treatment of leprosy in combination with rifampicin and clofazimine. It is so effective it is listed in the WHO's Model List of Essential Medicines.[28]

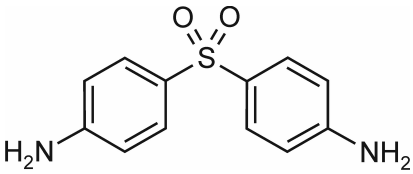

Figure 1. Molecular diagram of 4,4′-diaminodiphenyl sulfone (DDS, dapsone).

The compound has been reported to be polymorphic (anhydrate **Forms I** – **IV**), with form **III** being mentioned to be the most stable anhydrous form.[29, 30] A schematic diagram of the vapor pressure curves of the four modifications was constructed, indicating that the polymorphic pairs **II/III**, **III/I** and **II/I** are enantiotropically related. The enantiotropic relationship between the isosymmetric polymorphs **II** and **III** was reinvestigated by us very recently, providing a molecular level understanding of the highly reversible transformation.[31] Crystal structures of neat DDS solid forms have only be reported for Forms **III**[32-36] and **II**[31]. In addition to the anhydrous forms, crystal structures for a DDS hydrate with the unusual DDS:water stoichiometry of 3:1 (**0.33-Hy**)[37-39] and solvates with dichloromethane (hemi-), 1,4-dioxane and tetrahydrofuran (both monosolvates)[40, 41] have been published. During our investigations of the **0.33-Hy** we obtained a new anhydrous form, named **Form V**, which first emerged during water activity measurements (slurry method) as the only stable solid phase below a water activity of 0.64.[42] Repeating the slurry experiments (cycling in between 10 and 30 °C) in different organic non-solvate forming solvents (e.g., methyl isobutyl ketone, nitromethane, xylene, decanol, cyclohexane, *etc*.) also lead to **Form V**, indicating that **Form V** and not **Form III** is the most stable anhydrate polymorph of DDS at RT. Furthermore, the work on the **0.33-Hy** showed that it is possible to dehydrate the hydrate to an isomorphic dehydrate (**Hy$_{dehy}$**).[42]

In this study, we explore the structural, kinetic and thermodynamic relationships through a combination of experiment and theory [43, 44] between the five polymorphs and the isomorphic dehydrate as a function of temperature. A broad range of experimental techniques, including thermal analysis, solution calorimetry, solubility and gravimetric moisture sorption/desorption measurements and X-ray powder diffraction, along with crystal structure prediction and lattice energy modelling, are used to update previous results, quantify the phase stabilities, provide an atomistic level understanding of the phase interrelations (including a semi-schematic energy temperature diagram), and investigate why **Form V** was not found earlier.

2. Materials and Methods

2.1. Materials

Dapsone **Form III** (purity 97%) was purchased from Aldrich. The obtained sample was recrystallized from a hot-saturated methanol solution. The solid product was isolated by filtration and consisted of **Form III**. The organic solvents used were all of analytical grade and purchased from Aldrich or Fluka.

2.2. Thermal Analysis

Hot-Sage Microscopy. For HSM investigations a BH2 polarization microscope (Olympus, A), equipped with a Kofler hot-stage (Reichert, A), was used. Photographs were taken with an Olympus DP71 digital camera.

Differential Scanning Calorimetry. DSC thermograms were recorded on a DSC 7 or Diamond DSC (Perkin-Elmer Norwalk, Ct., USA) controlled by the Pyris 7.0 software. Using a UM3 ultramicrobalance (Mettler, Greifensee, CH), samples of approximately 2 – 10 mg were weighed into perforated/sealed aluminum capsules. The samples were heated using rates in between 2 and

10 °C min^{-1}, with dry nitrogen as the purge gas (purge: 20 ml min^{-1}). The two instruments were calibrated for temperature with pure benzophenone (mp 48.0 °C) and caffeine (236.2 °C), and the energy calibration was performed with indium (mp 156.6 °C, heat of fusion 28.45 Jg^{-1}). The errors on the stated temperatures and enthalpy values were calculated at the 95% confidence intervals and are based on at least three measurements.

2.3. Solution Calorimetry

The experiments were performed with the TAM III nanocalorimeter unit (TA Instruments, Eschborn, Germany). Solution calorimetry data were recorded using a [3220]-20 mL micro solution ampoule. The experiments were performed at 25 °C in 15 mL of DMSO and methanol. Approximately 10 to 15 mg of sample was accurately weighed into reusable stainless steel capsules using a UM3 ultramicrobalance (Mettler, Greifensee, Switzerland). Once the baseline had stabilized to ± 50 nW, the capsule was dropped into the calorimeter. The heat flow into or out of the calorimeter was recorded and data analysis performed using the TAM Assistant software. The heat flow of the empty RH capsule was subtracted from the heat flow of the sample measurements. The errors on the stated enthalpy values are calculated at the 95% confidence intervals and are based on at least three measurements. The calorimeter was calibrated periodically using the electrical substitution method, as well as with reference materials (KCl and sucrose).

2.4. Determination of Solubility

The Crystal16 crystallization system (Technobis, NL) was used to determine the solubilities of **Forms III** and **V** in water. The temperature at the point the suspension becomes a clear solution upon heating or “clear point” (at 0.1 °C per minute) was taken as the saturation temperature of the measured sample with known concentration. To make sure that solvent-mediated transformations had not occurred during the measurements, an excess amount of solid was stirred under the same

conditions and PXRD patterns of the residual solid were recorded after reaching the highest clear point temperature derived from the solubility experiments.

2.5. Gravimetric Moisture Sorption/Desorption Experiments

Moisture sorption and desorption studies (GMS) were performed with the automatic multisample gravimetric moisture sorption analyzer SPS23-10µ (ProUmid, Ulm, D). The moisture sorption analyzer was calibrated with saturated salt solutions according to the supplier's recommendations. Approximately 250 mg of sample was used for each analysis. The measurement cycles were started at 40% RH with an initial stepwise desorption (decreasing humidity) to 0 %, followed by a sorption cycle (increasing humidity) to 90% RH and a final sorption step to 0% RH. RH changes were set to 5% for all sorption/desorption steps. The equilibria conditions for each step were set to a mass constancy of ± 0.001 % over 60 minutes and a maximum time limit of 48 hours.

2.6. Powder X-ray Diffraction

PXRD patterns for characterizing the DDS solid forms were obtained using an X'Pert PRO diffractometer (PANalytical, Almelo, NL) equipped with a θ/θ coupled goniometer in transmission geometry, programmable XYZ stage with well plate holder, Cu-K$\alpha_{1,2}$ radiation source with a focusing mirror, a 0.5° divergence slit and a 0.02° Soller slit collimator on the incident beam side, a 2 mm antiscattering slit and a 0.04° Soller slit collimator on the diffracted beam side and a solid state PIXcel detector. The patterns were recorded at a tube voltage of 40 kV and tube current of 40 mA, applying a step size of $2\theta = 0.013°$ with 40 s, 80 s or 200 s per step in the 2θ range between 2° and 40°.

PXRD data for solving **Form V** were collected on a STOE STADIP transmission diffractometer using monochromatic Cu-K$_{\alpha 1}$ radiation (1.54056 Å) at 40kV, 30mA from a focusing Ge(111)

primary beam monochromator and a Mythen1k detector with an 18° 2θ angular range. The sample was mounted in 0.7mm borosilicate glass capillary and rotated in the beam during collection. Four data-sets were collected and summed together, each from 2 to 70° 2θ stepping at 0.1° and 15 seconds a step and a data-step of 0.15° 2θ.

Form V[§] indexed to a monoclinic unit cell, $P2_1/n$, with Z'=4. The data were background subtracted and truncated to 36.78° 2θ for Pawley fitting.[45] Simulated annealing was used to optimize the DDS model against the diffraction data set in direct space. The internal coordinate (*Z*-matrix) description was derived from the PBE-TS optimized **Form III** structure, with C–H distances normalized to 0.95 Å. The structure was solved using 250 simulated annealing runs of 5×10^8 moves per run as implemented in DASH, allowing 24 external and 8 internal degrees (SO_2–phenyl dihedrals) of freedom. The best solutions returned a χ^2 ratio of *ca*. 3.71 (profile χ^2/ Pawley χ^2). This solution was then optimized using CASTEP (for settings see section 2.7), with the lattice parameters fixed to the experimentally determined values. The minimized structure was then used as an input for Rietveld refinement, 2θ range 3.0 to 69.95°, using TOPAS academic V5.[46] The geometry of each molecule was defined by a rigid body. Rotation and translation parameters were simultaneously refined with the SO_2–phenyl dihedrals of each independent molecule in the asymmetric unit. The background was modelled by a set of consecutive points with refinable intensities. The isotropic temperature factor (B_{iso}) for non-hydrogen atoms refined to 3.77(8) and for hydrogen atoms to 1.2 • 3.77(8). The final refinement included a total of 79 parameters (26 profile, 4 cell, 1 scale, 15 preferred orientation, 1 isotropic temperature factor and 32 position). The refinement converged at R_{wp} = 2.38%, R_{exp} = 1.64%, R_p = 1.87% (Figure 2). The experimental structure and optimized structure (lattice parameters fixed to experimental values) are in excellent agreement ($rmsd_{30}$ = 0.04 Å, Figure S3 of the Electronic Supporting Information).

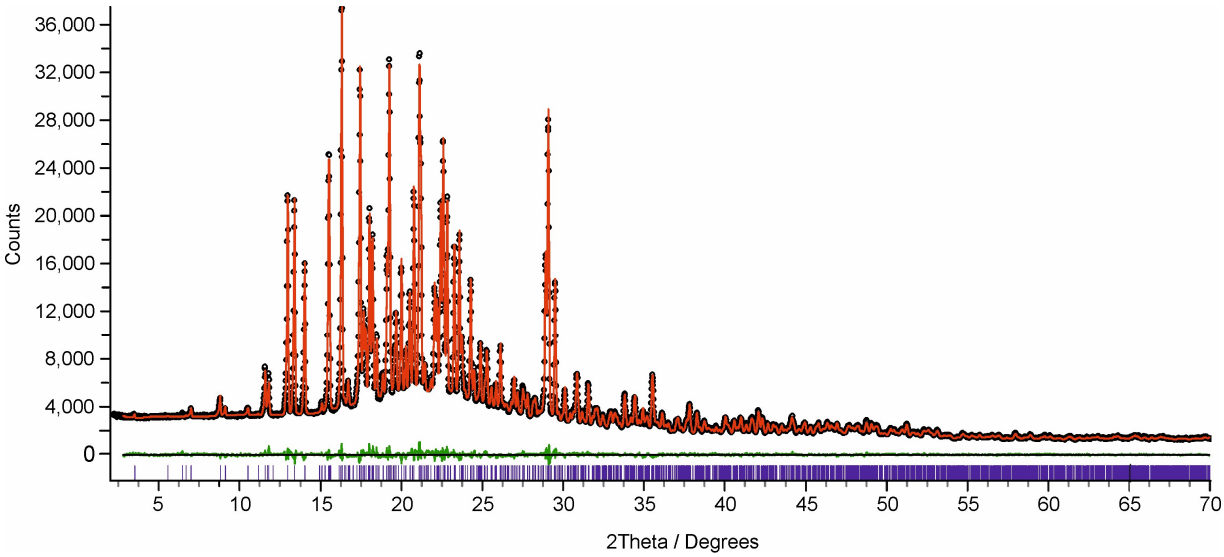

Figure 2. Observed (black points), calculated (red line) and difference (green line) profiles for the Rietveld refinement of **Form V**. Blue tick marks denote the peak positions.

The resulting structure from the Rietveld refinement was further scrutinized by allowing all fractional coordinates to refine freely (395 parameters, R_{wp} = 1.77%). As expected, the improvement (R_{wp}) came at the expense of some chemical sense (e.g. slight distortion in planarity of the benzene rings, movement of H atoms to nonsensical positions), but otherwise, the geometry of the independent molecules was well preserved, supporting the accuracy of the rigid body refined crystal structure.

2.7. Computational Generation of the DDS Anhydrate Crystal Energy Landscape

Hypothetical crystal structures of DDS Z′=1 and Z′=2 anhydrates, starting from the PBE0/6-31G(d,p) optimized molecular conformation, calculated using Gaussian09,[47] were generated with the program CrystalPredictor.[48-51] 150,000 Z′=1 and 500,000 Z′=2 structures were generated randomly in 48 space groups (*P*1, *P*$\bar{1}$, *P*2$_1$, *P*2$_1$/*c*, *P*2$_1$2$_1$2, *P*2$_1$2$_1$2$_1$, *Pna*2$_1$, *Pca*2$_1$, *Pbca*, *Pbcn*, *C*2/*c*, *Cc*, *C*2, *Pc*, *Cm*, *P*2$_1$/*m*, *C*2/*m*, *P*2/*c*, *C*222$_1$, *Pmn*2$_1$, *Fdd*2, *Pnna*, *Pccn*, *Pbcm*, *Pnnm*, *Pmmn*, *Pnma*, *P*4$_1$, *P*4$_3$, *I*$\bar{4}$, *P*4/*n*, *P*4$_2$/*n*, *I*4/*m*, *I*4$_1$/*a*, *P*4$_1$2$_1$2, *P*4$_3$2$_1$2, *P*3$_1$, *P*3$_2$, *R*3, *P*$\bar{3}$, *R*$\bar{3}$, *P*3$_1$21, *P*322$_1$,

*R*3c, $R\bar{3}c$, $P6_1$, $P6_3$, $P6_3/m$), keeping the molecular geometry rigid. The structures were relaxed to a local minimum in the intermolecular lattice energy, calculated from the FIT[52] exp-6 repulsion-dispersion potential and atomic charges which had been fitted to the electrostatic potential around the PBE0/6-31G(d,p) charge density using the CHELPG scheme.[53] The energies of all structures within 36.5 kJ mol^{-1} and 15 kJ mol^{-1}, for Z′=1 and Z′=2, respectively, of the global lattice energy minimum were refined (ca. 20,000 structures), using DMACRYS[54] with a more realistic, distributed multipole model[55] for the electrostatic forces which had been derived using GDMA2[56] to analyze the PBE0/6-31G(d,p) charge density.

The optimal proton positions of the amino group and orientation of the phenyl groups, in all crystal structures within 20 kJ mol^{-1} (Z′=1) / 15 kJ mol^{-1} (Z′=2) of the global minimum (1691 structures), were determined using the CrystalOptimizer database method.[57] This was done by minimizing the lattice energy (E_{latt}), calculated as the sum of the intermolecular contributions (U_{inter}) and the conformational energy penalty paid for distortion of the molecular geometry to improve the hydrogen bonding geometries. Conformational energy penalties (ΔE_{intra}, with respect to the pyramidal global conformational energy minimum) and isolated molecule charge densities were computed at the PBE0/6-31G(d,p) level, for each conformation considered in the minimization of E_{latt}. All isolated-molecule wave function calculations were performed using Gaussian09[47] and intermolecular lattice energies using DMACRYS.[54]

The most stable anhydrates [239 structures, 20 kJ mol^{-1} (Z′=1) / 17 kJ mol^{-1} (Z′=2) with respect to the global minimum] were optimized with periodic density functional calculations (CASTEP [58]). The Perdew-Burke-Ernzerhof (PBE) generalized gradient approximation (GGA) exchange-correlation density functional[59] and ultrasoft pseudopotentials,[60] with the addition of the Tkatchenko and Scheffler (TS)[61] semi-empirical dispersion correction, were applied. The number

of *k*-points were chosen to provide a maximum spacing of 0.07 $Å^{-1}$ and a basis set cut-off of 780 eV was applied. The optimizations were considered complete when energies were converged to better than $2x10^{-5}$ eV per atom, atomic displacements converged to $1x10^{-3}$ Å, maximum forces to $5x10^{-2}$ eV $Å^{-1}$, and maximum stresses were converged to 0.1 GPa. The lattice energies of the structures within 20 kJ mol^{-1} of the lowest energy structure were recalculated, without optimization, using the same settings, but the D2[62] dispersion correction. Isolated molecule minimizations to compute the isolated DDS energy (U_{gas}) were performed by placing a single molecule/ion in a fixed cubic 35x35x35 $Å^3$ unit cell, then optimized with the same settings as used for the crystal calculations.

The initial rigid-body search missed the **Form II** structure (which is isosymmetric and enantiotropically related to **Form III**, with **Form III** being more stable at 0 K[31]). Therefore, the CrystalPredictor search for DDS structures was repeated in $P2_12_12_1$ using the experimental **Form II** conformation (slight difference in the NH_2 orientations). The 10 lowest energy structures were then optimized using CASTEP, with the lowest of the structure corresponding to **Form II**. Furthermore, **Forms V** (Z'=4), **Hy_{dehy}** (Z'=1) and alternative **Form IV** structures (in P1, Z'=8) were optimized using CASTEP, with the same setting as described for the search.

3. Results

3.1. Production and Specification of the Crystal Forms

Form I is the high temperature form of DDS and can be produced by annealing the melt of any solid form at temperatures above 170 °C, preferentially in the presence of **Form I** seeds. The latter is often the case if a solvate form (**0.33-Hy** or solvate) is used as starting material, i.e. **Form I** seeds are produced upon desolvation. The maximum growth rate of **Form I** from the melt was

observed below 170 °C, however, also **Form II** was found to nucleate and grow at that temperature. We were not able to crystallize the high temperature **Form I** directly from solvents.

Form II, which is enantiotropically related to **form III**, exists only at temperatures above ca. 74 °C. The 1st order **III** ↔ **II** phase transformation occurs at 78 ± 4 °C.[31] Desolvation of the solvates at temperatures above the **III** → **II** transition point resulted in **Form II** with **Form I** impurities. Furthermore, **Form II** can be produced from the melt. The maximum formation rate of **Form II** from the melt was observed around 120 °C.

Evaporation and cooling crystallization experiments from all solvents, with the exception of solvate-forming solvents, lead to **Form III**. Desolvation of the DDS solvates at temperatures < 75 °C resulted in **Form III** with **Form I** impurities.

Annealing the quench cooled melt of DDS at 50 – 70 °C induces the concomitant crystallization of the **Forms III** and **IV**. Interestingly, starting with the **0.33-Hy**, the amount of **Form IV** was enriched in melt crystallization experiments. Similar to **Form I** we were not able to crystallize **Form IV** directly from solvents.

Form V is obtained when slurring any DDS solid form in non-solvate forming solvents in the temperature range 10 to 90 °C and in water/organic solvent mixtures at water activities (a_w) < 0.64 at room temperature (RT).

Starting from **0.33-Hy**, which was prepared according to procedures described an earlier report,[42] the isomorphic dehydrate can be produced by storing the hydrate at driest conditions at room temperature (RT).

3.2. Temperature Induced Phase Transformations

Hot-stage microscopy (Figure 3) and differential scanning calorimetry (Figure 4) were applied to reinvestigate the reported temperature induced transformations of **Forms I–IV**[29] and to complete the results with measurement data for **form V** and **Hy**$_{dehy}$. The thermochemical data are summarized in Table 1.

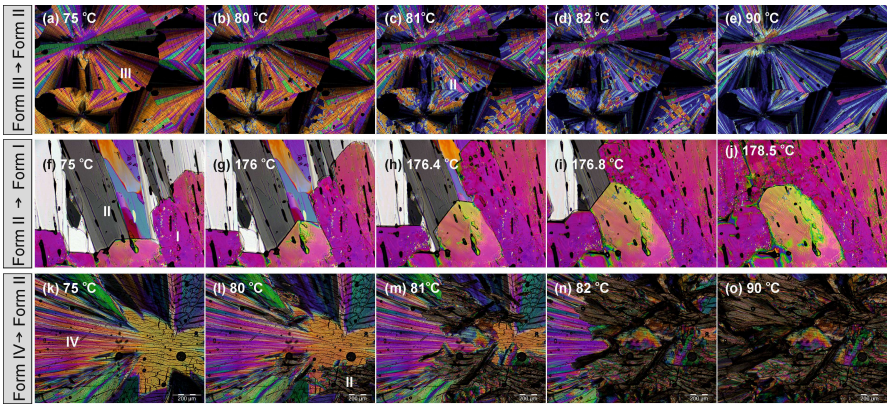

Figure 3. Polarized-light photographs showing selected temperature induced solid-state transformations of DDS (**III** → **II**, **II** → **I** and **IV** → **II**).

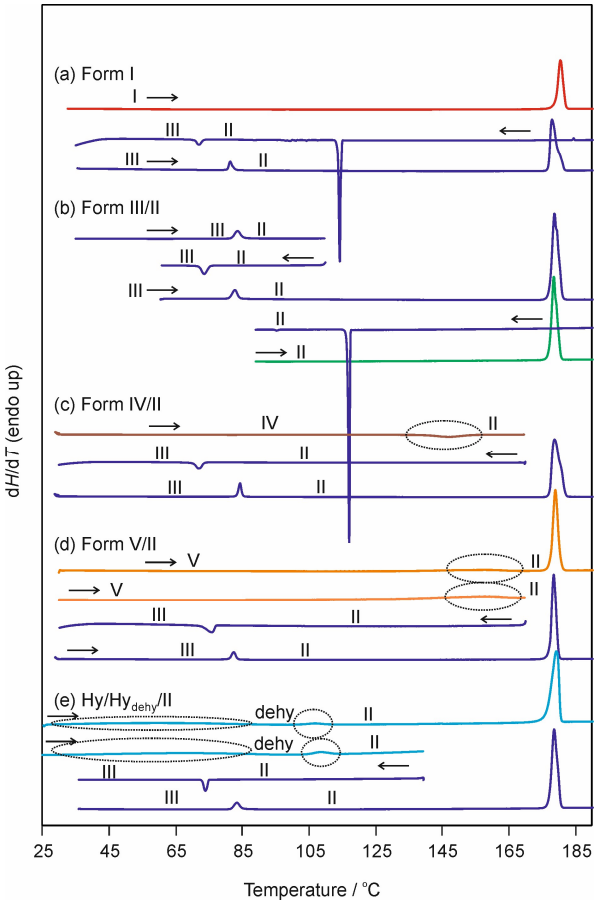

Figure 4. DSC curves of DDS solid forms (polymorphs **I** to **V**, **0.33-Hy** and **Hy$_{dehy}$**) recorded at a hating rate of 10 kJ mol^{-1}. Arrows indicate the course of the experiments (*i.e.*, heating and cooling) and encircled with dashed lines are transformation reactions.

Table 1. Physicochemical data for DDS solid forms.

Form	**I**	**II**	**III**	**IV**	**V**	**Hy_{dehy}**	**0.33-Hy**
Thermal Analysis							
T_{fus}[a] / °C	179.1 ± 0.1	177.2 ± 0.1		~ 170[29]			
$\Delta_{fus}H$[b] / kJ mol^{-1}	18.60 ± 0.22	21.40 ± 0.05	23.46 ± 0.08[g]	≤ 18.43 ± 0.19[g]	24.11 ± 0.20[g]	22.49 ± 0.07[g]	
$\Delta_{trs}H$[c] / kJ mol^{-1} (x → y)		–2.02 ± 0.07 (II → III)	2.06 ± 0.06 (III → II)	–2.97 ± 0.18 (IV → II)	2.70 ± 0.19 (V → II)	1.08 ± 0.05[42] (Hy_{dehy} → II)	2.95 ± 0.09[42] (Hy → Hy_{dehy}) 4.03 ± 0.10[42] (Hy → II)
$\Delta_{trs}H$[c] / kJ mol^{-1} (x → Form V)	–5.50 ± 0.30	–2.70 ± 0.21	–0.64 ± 0.20	–5.68 ± 0.27	0	–1.62 ± 0.21	
Order of thermodynamic stability at 0 K	e	d	b	f (lowest)	a (highest)	c	
Solubility Measurements (Water)							
$\Delta_{sol}H$[d] / kJ mol^{-1}			25.3		26.6		
$\Delta_{trs}H$[c]/ kJ mol^{-1} (x → Form V)			–1.4		0		
Order of thermodynamic stability at 0 K			b		a		
$\Delta_{sol}S$[e] / kJ mol^{-1}			32.3		34.6		
Solution calorimetry (DMSO and MeOH)							
$\Delta_{sol}H_{DMSO}$[d] / kJ mol^{-1}			–14.20 ± 0.08		–13.92 ± 0.04		
$\Delta_{trs}H$[c] / kJ mol^{-1} (x → Form V)			0.23 ± 0.09		0		
$\Delta_{sol}H_{MeOH}$[d] / kJ mol^{-1}			13.74 ± 0.07		13.88 ± 0.06		
$\Delta_{trs}H$[c] / kJ mol^{-1} (x → Form V)			0.14 ± 0.09		0		
Order of thermodynamic stability at 0 K			b		a		
Lattice Energy Calculations							
PBE-TS E_{latt}[f] / kJ mol^{-1}	–194.52	–194.92	–198.16	–189.68[h]	–200.54	–197.26	
ΔE_{latt} / kJ mol^{-1}	6.02	5.62	2.38	10.86	0	3.29	
PBE-D2 E_{latt}[f] / kJ mol^{-1}	–194.61	–195.09	–198.21	–189.80[h]	–198.53	–196.72	
ΔE_{latt} / kJ mol^{-1}	3.92	3.44	0.32	8.82	0	1.81	
Order of thermodynamic stability at 0 K	e	d	b	f	a	c	

[a] T_{fus} – melting temperature, [b] $\Delta_{fus}H$ – enthalpy of fusion, [c] $\Delta_{trs}H$ – enthalpy of transition, [d] $\Delta_{sol}H$ – enthalpy of solution, [e] $\Delta_{sol}S$ – entropy of solution, [f] E_{latt} – lattice energy, [g] calculated by applying the Hess's law, [h] for Form **IV** an ordered version of the structure was used for the calculations.

The DSC trace of **Form I** shows only one thermal event (Figure 4a), the melting of the neat form at 179.1 ± 0.1 °C with a heat of fusion ($\Delta_{fus}H_I$) of 18.60 ± 0.22 kJ mol^{-1}. Upon cooling the melt (10 °C min $^{-1}$), spontaneous recrystallization of **Form II** is observed at temperatures < 125 °C. The exothermic **Form II → Form III** phase transformation occurs at approx. 75 °C (–2.02 ± 0.07 kJ mol^{-1}), upon further cooling the sample. Reheating the sample or staring from a **Form III** batch (Figure 4b) shows the endothermic **Form III → Form II** solid-solid transformation at temperatures slightly above 80 °C (Figure 3a-e), confirming the enantiotropic relationship[63, 64] of the polymorphic pair **Form II/III**. The measured onset temperatures and heat of transformations (2.06 ± 0.06 kJ mol^{-1}) are in excellent agreement with our previous results.[31] The melting point of **Form II** was recoded at 177.2 ± 0.1 °C. The melting peak of **Form II** exhibits a shoulder, which can be related to the melting of **Form I**, which crystallizes during melting of **Form II**. Figure 3f-j show the **Form II** to **Form I** transformation recorded slightly below the melting of **Form II**. The heat of fusion of **Form II** was measured as 21.40 ± 0.05 kJ mol^{-1}.

Figure 4c shows the DSC trace of DDS **Form IV**, prepared by quench cooling the DSC pan to RT followed by annealing the sample for 15 minutes at 60 – 70 °C. The absence of the **Form III** to **Form II** transformation peak confirms that only **Form IV** was present. Heating **Form IV** to temperatures above 125 °C induces the phase transformation into **Form II** (Figure 3k-o). The pronounced changes in texture during the transformations observed by HSM (Figure 3) indicate that in comparison to the **Form II → III** transformation (isosymmetric polymorphs), a greater structural difference can be expected between **Forms II** and **IV**, as well as **Forms II** and **I**. The DSC investigations allowed us to quantify the heat of **Form IV → II** transformation as –2.97 ± 0.18 kJ mol^{-1}. This exothermic event on heating is a clear indication that the polymorphic pair

IV/II is monotropically related.[63, 64] Additionally, it was observed that within few days the metastable **Form IV** transformed to **Form III** at RT.

The new polymorph, **Form V**, shows an endothermic transformation reaction to **Form II** at temperatures above 145 °C with a transformation enthalpy (**Form V → Form II**) of 2.70 ± 0.19 kJ mol^{-1}. Finally, the isomorphic dehydrate (**Hy$_{dehy}$**) of **0.33-Hy**, prepared by dehydrating the hydrate *in-situ* (Figure 4e), shows the transformation to **Form II** at temperatures above 100 °C. The **Hy$_{dehy}$** to **Form II** transformation enthalpy was estimated to be 1.08 ± 0.05 kJ mol^{-1}, indicating that the dehydration product **Hy$_{dehy}$** is more stable than the **Forms I**, **II** and **IV** at 0 K.

The fact that **Form V** shows a higher transition enthalpy to **Form II**, than form at RT (**III**), indicates that **Form V** is more stable than **Form III**, which was considered as being the most stable form of DDS to date.

3.3. Solubility Experiments and Heat of Solution Measurements of Forms III and V

The two anhydrates (**III** and **V**) show an appreciable stability in the solid state at ambient storage conditions. Both, phase pure **Forms III** and **V** were stable for at least six and two years (end of investigation time), respectively. The stability order of the two stable anhydrate forms was therefore qualitatively estimated as a function of temperature from Crystal16 parallel reactor system solubility measurements in water (Figure 5a). The measurements are in reasonable agreement with previous solubility studies of DDS **Form III** in water.[65, 66] **Form V** shows a lower solubility than **Form III** confirming that **Form V** is the thermodynamically stable polymorph in the investigated temperature range. The solubility data plotted in van't Hoff form show no signs of convergence or crossover below the DDS melting temperature (Figure 5b). Based on the

extrapolated intersection of the van't Hoff plots the transition point between the two anhydrous forms lies around 323 °C, well above the melting point of DDS.

The enthalpy of solution (ΔH_{sol}) and entropy of solution (ΔS_{sol}) were estimated from the slope and intercept of the regression line of the van't Hoff plot, respectively (Table 1, Figure 5b). The enthalpies and entropies of solution are positive for the two forms and greater for **Form V** than **Form III**. The enthalpy difference between the two forms was estimated as 1.4 kJ mol^{-1}.

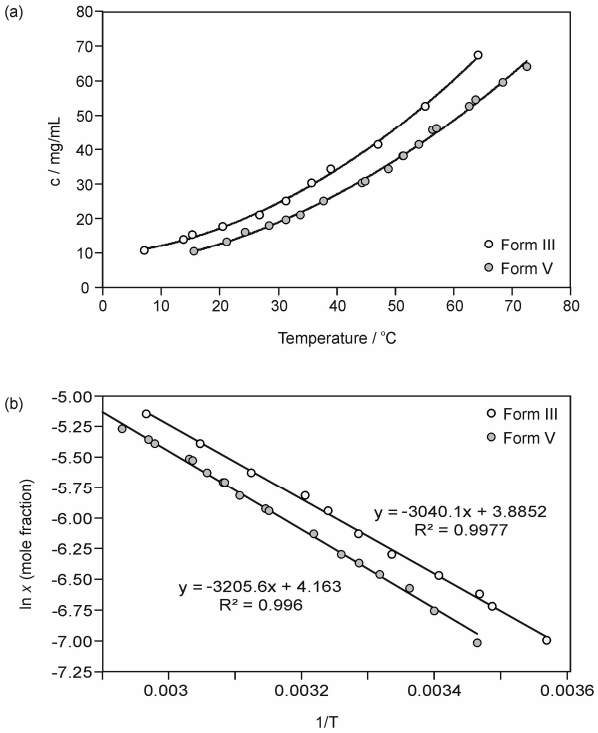

Figure 5. (a) Solubility (mg mL^{-1}) of DDS **Forms III** and **V** in water as a function of temperature and (b) van't Hoff plot of the molar solubility as a function of temperature.

Solution calorimetry experiments were performed to confirm the stability order between **Forms III** and **V**. Heat of solutions of the two polymorphs were measured in DMSO and MeOH and in both cases the enthalpy of solution was slightly higher for **Form V** than for **Form III**, resulting in

an energy difference of 0.23 ± 0.09 kJ mol^{-1} and 0.14 ± 0.09 kJ mol^{-1} in DMSO and MeOH, respectively (Table 1). The DSC, solubility and solution calorimetry results consistently indicate that **Form V** is more stable than **Form III**, albeit the enthalpic stabilization of **Form V** with respect to **Form III** is low (< 1 kJ mol^{-1} as derived from DSC and solution calorimetry experiments).

3.4. Moisture Sorption/Desorption Analysis of Form III and Form V, Water Activity Measurements (Slurry Method) and Long-Time Stability Experiments

Forms III and **V** were subjected to automated moisture sorption/desorption studies at 25 °C. The two anhydrates show practically no water uptake (< 0.03 %) up to 90% RH (Figure 6). No transformation to the **0.33-Hy** was observed and based on the sorption/desorption data both anhydrate phases can be classified as non-hygroscopic.[67]

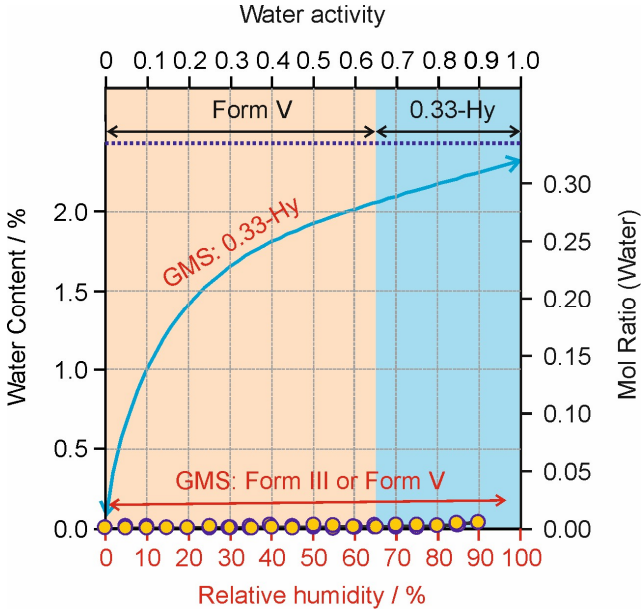

Figure 6. Kinetic (GMS) and thermodynamic (water activity measurements) stability of DDS **Forms III**, **V** and **0.33-Hy** at 25 °C. The yellow circles indicate the GMS equilibrium measurement points (see section 2.5) for **Forms III** and **V** (superimposable). The bent blue arrow indicates the course of the GMS data recorded for **0.33-Hy**.[42] Results from water activity measurements (slurry method) are indicated by color-code in the background of the figure (critical water activity ~ 0.65).

In order to overcome the kinetic control governing the gravimetric moisture sorption/desorption studies, water activity measurements (slurry method) were performed in a previous study[42] and the results contrasted to the GMS data. The water activity measurements at 25 °C showed that at an $a_w > 0.66$, **0.33-Hy** is the stable form and at $a_w \leq 0.64$ **Form V** is the thermodynamically most stable form, suggesting that the hydrate is the stable form at high water activities and that the equilibrium between the **Form V** and the **0.33-Hy**, lies at an a_w value of ~0.65 at 25°C (Figure 6).[42]

Additional slurry experiments were performed at low a_w values ($a_w \leq 0.3$) in the temperature range 10 – 90 °C using either **Form III** or **Form V** or a 1:1 mixture of the two compounds as a starting material. **Form V** was confirmed as the stable phase, however, the transformation of **Form III** into **Form V** was found to be very slow. After three weeks (end of investigation time) **Form III** was still detectable in several samples, albeit the amount obviously decreased.

Long-time stability data could be derived for a DDS sample, consisting of a mixture of **Form III** and **0.33-Hy**,[29] which had been stored for over 40 years at ambient conditions. After four decades the sample is still a mixture of the two solid forms, clearly indicating that both, **Form III** and **0.33-Hy** show a very high kinetic stability as no transformation to **Form V** occurred.

3.5. Thermodynamic Stability of DDS Anhydrous Forms

The relative stability order of a complex polymorphic systems can be unraveled based on the heat of fusion as well as the heat of transformation rule and a semi-schematic energy-temperature diagram allows to graphically outline the thermodynamic relationships of all polymorphs (Figure 7).[63, 64, 68] For **Forms I** and **II** it is possible to directly measure the fusion temperatures (T_{fus}, Table 1) and enthalpies of fusion ($\Delta_{fus}H$). The melting point of **Form IV** could be determined using faster

heating rates in HSM investigations to be ~ 170 °C, in agreement with a previous report.[29] For the remaining two polymorphs, **Forms III** and **V**, the melting points could not be determined. However, we were able to measure the transition enthalpies ($\Delta_{trs}H$) for the polymorphic pairs **III**/**II**, **IV**/**II**, **V**/**II** and **Hy$_{dehy}$**/**II** (Table 1) and, thus, by applying Hess's law of heat of summation the heat of fusions of **Forms III**, **IV** and **V** can be calculated (Table 1). Based on the heats of fusion the 0 K stability order of the polymorphs and **Hy$_{dehy}$** can be derived as follows: **V** (most stable) > **III** > **Hy$_{dehy}$** > **II** > **I** > **IV** (least stable).

Considering only the true polymorphs (**Forms I** – **V**), this results in 10 pairs of polymorphs which can be either monotropically or enantiotropically related. In case a pair has been determined to be enantiotropic, the transition temperature becomes of great interest. It is possible to estimate the transition temperature from the measured melting points and heat of fusions (eq. 1),[63, 64, 69-71]

$$T_{trs} = \frac{\Delta_{fus}H_2 - \Delta_{fus}H_1 + (C_{p,liq} - C_{p,1}) \cdot (T_{fus,1} - T_{fus,2})}{\frac{\Delta_{fus}H_2}{T_{fus,2}} - \frac{\Delta_{fus}H_1}{T_{fus,1}} + (C_{p,liq} - C_{p,1}) \cdot \ln(\frac{T_{fus,1}}{T_{fus,2}})} \qquad \text{(eq. 1)}$$

where T_{trs} is the thermodynamic transition point, T_{fus} the melting point, $\Delta_{fus}H$ the heat of fusion and Cp the heat capacity. The indices 1 and 2 stand for the higher and lower melting form, respectively. Since heat capacities of the melt ($C_{p,liq}$) and the higher melting form ($C_{p,1}$) are usually not available, an empirical correction term $k\,\Delta_{fus}H_1$ can be used for the heat capacity difference $C_{p,liq}$–$C_{p,1}$. Typical empirical values for k range from 0.001 to 0.007 K^{-1} with an average of k = 0.003 K^{-1} (eq. 2).[69]

$$T_{trs} = \frac{\Delta_{fus}H_2 - \Delta_{fus}H_1 + k \cdot \Delta_{fus}H_1 (T_{fus,1} - T_{fus,2})}{\frac{\Delta_{fus}H_2}{T_{fus,2}} - \frac{\Delta_{fus}H_1}{T_{fus,1}} + k \cdot \Delta_{fus}H_1 \cdot \ln(\frac{T_{fus,1}}{T_{fus,2}})} \qquad \text{(eq. 2)}$$

Furthermore, transforming (eq. 1) and (eq. 2) allows us to estimate an unknown melting point from the heat of transition, transition point and melting data (eq. 3).

$$T_{fus,2} = \frac{\Delta_{fus}H_2 \cdot T_{fus,1} \cdot T_{trs})}{T_{fus,1} \cdot \Delta_{fus}H_2 + T_{trs} \cdot \Delta_{fus}H_1 - T_{fus,1} \cdot \Delta_{fus}H_1} \qquad \text{(eq. 3)}$$

Applying eq.3 it is possible to estimate the melting point of **Form III** (~ 166 °C), indicating that it is lower than the melting point of **Form IV.** The calculated (eq. 2) transition points between the polymorphic pairs **III/II** (T_{trs} ~ 80 °C), **III/I** (~ 130 °C), **III/IV** (~ 154 °C) and **II/I** (~ 165 °C) resulted in values smaller than the melting points of the forms and thus confirm an enantiotropic relationship between the four pairs of polymorphs. As the DSC heating experiments of **Form V** show an endothermic transition into **Form II** (Figure 4d), we can conclude that the pair **V**/**II** is also enantiotropically related with the transition point being below 145 °C. Knowing that the free energy curves of the Forms **V** and **II** must intersect below 145 °C, we can derive that the pair **V**/**I** is also enantiotropically related as becomes obvious from the courses of the free energy curves in the semi-schematic energy temperature diagram. For the pairs **V**/**III** and **V**/**IV** the measured (thermal) data do not allow us to conclude on the type of interrelation, however, the solubility data indicated a monotropic relationship for forms **III** and **V**, which implies that **Form V** is also monotropically related to **Form III** and that its melting point lies somewhere between that of the **Forms IV** and **I**. More important, from Figure 7 it can be concluded that **Form V** is the thermodynamically most stable form at low, room and slightly elevated temperatures (at least up to 90 °C as derived from slurry experiments). **Form II** is the thermodynamically stable form in a temperature window between the transition temperature of **V** to **II** (> 90 °C) and **II** to **I** (~ 165 °C) and finally **Form I** is the most stable form at temperatures > 165 °C and its melting point.

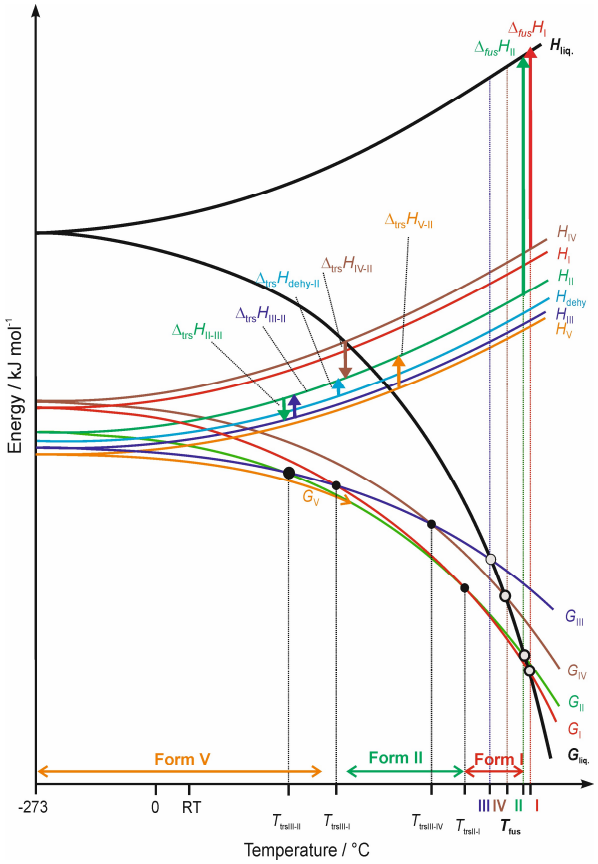

Figure 7. Semi-schematic energy/temperature diagram of DDS polymorphs and **Hy$_{dehy}$** (*H* curve only). T_{fus}, melting point; *G*, Gibbs free energy; *H*, enthalpy; $\Delta_{fus}H$, enthalpy of fusion; T_{trs}, transition point; $\Delta_{trs}H$, transition enthalpy; liq, liquid phase (melt). The bold vertical arrows signify experimentally measured enthalpies, and the horizontal double arrows mark temperature ranges where either **Form V**, **II** or **I** is the thermodynamically stable form.

Our findings concerning the thermodynamic interrelationship between the DDS polymorphs are in line with the schematic vapor pressure temperature diagram of **Forms I – IV** suggested by Kuhnert-Brandstätter et al. (Figure S4 of the Electronic Supporting Information),[29] and complement the existing knowledge with new forms (**From V, Hy$_{dehy}$**) and the perception that the relationship of the pair **III**/**IV** is enantiotropic.

3.6. Structural Features - Experimental and Thermodynamically Feasible DDS Structures

Anhydrate structures are known for Forms **II**[31] and **III**.[32-36] Furthermore, the **0.33-Hy** structure[37-39] has been determined, which is isostructural to $\mathbf{Hy_{dehy}}$. Due to the fact that **Forms I**, **IV** and **V** were never obtained in solution crystallization experiments, PXRD and crystal structure prediction (CSP) were chosen to derive the structures.

3.6.1. Forms II, III and V

Form V was successfully solved from PXRD data (Figure 2). The thermodynamically most stable form at low and room temperature crystallizes in the monoclinic space group $P2_1/n$, with $Z'=4$. Three of the four independent DDS molecule conformations in **Form V** are closely related to the DDS gas phase conformation, differing by 2.8 to 4.5 kJ mol^{-1} in intramolecular energy (ΔE_{intra}) with respect to the PBE/6-31G(d,p) global energy minimum conformation. The fourth crystallographically independent DDS molecule adopts a distorted molecular conformation, with an ΔE_{intra} of 14.7 kJ mol^{-1} (Figure 8). Lattice energy optimizations starting from the experimental **Form V** structure and a hypothetical **Form V** model in which all four DDS molecules adopt a conformation related to the gas phase minimum resulted in two distinct energy minima, with the experimental structure being stabilized by –11.8 kJ mol^{-1}. Thus, intermolecular energy contributions in **Form V** outweigh the ΔE_{intra} penalty (14.7/4 kJ mol^{-1}) seen in one of the four DDS molecules in the experimental structure. Disorder modelling of the "distorted" conformation neither improved the PXRD fit nor the stability of the structure (lattice energy).

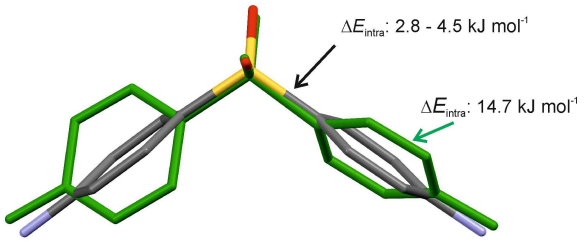

Figure 8. Overlay of the two distinct experimental conformations observed in DDS **Form V**. Color-coded the conformation observed for three of the symmetry independent DDS molecules. The fourth and distinct conformation is depicted in green. Intramolecular energy penalties are given.

Comparing the packings of the experimental DDS solid forms reveals that **Form V** is structurally related with the two isosymmetric DDS structures **Forms II** and **III** (Figure 9). In all three structures the SO_2 groups act as acceptors for N–H···O hydrogen bonding interactions and together with N–H···N hydrogen bonds the 3D H-bonded network structures are formed.[31] In **Forms III** and **II** the DDS molecules form layers which are the stacked along the *b* crystallographic axes, similar layers are also seen in **Form V**.

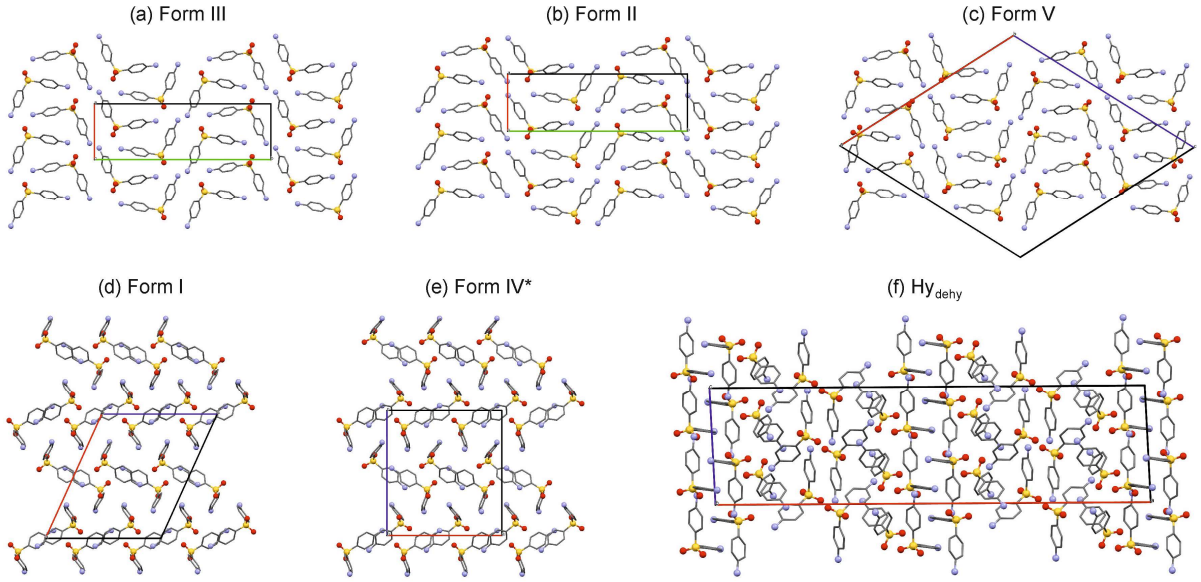

Figure 9. Packing comparisons of the DDS solid forms, viewed along the crystallographic axes *c* (a,b) or *b* (c-f). For **Form IV** an ordered structure model is shown.

There is much more diversity to the crystal packing of **Form V** and the structures of **Forms II** and **III** than suggested in Figure 9a-c. A closer inspection of the arrangement of DDS molecules within the layers reveals the differences between **Form V** and the other two structurally related

polymorphs. In **Forms II** and **III** the molecules are solely related by 2_1 symmetry, whereas in **Form V** the four independent molecules adopt slightly different positions (leading to Z′=4) and more important are not related by 2_1 symmetry but by glide plane symmetry, leading to upside-down orientations of half of the DDS molecules (Figure 10).

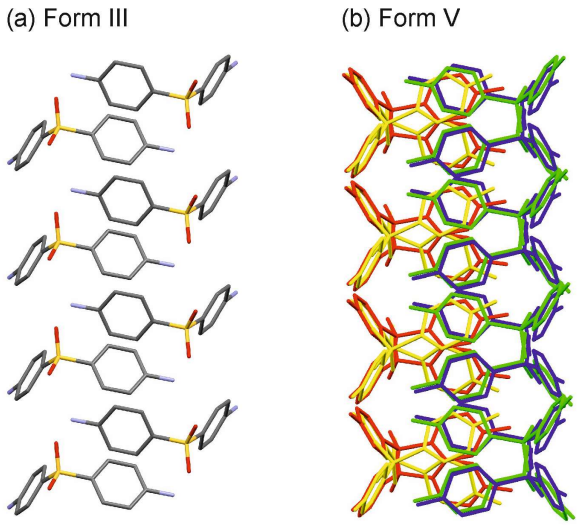

Figure 10. Comparison of DDS **Form III** (a) and **V** layers (b) viewed along the *a* crystallographic axis (a) and *ab* (b). Symmetry independent molecules are color-coded in (b).

3.6.2. Computationally Generated Anhydrate Crystal Energy Landscape

The DDS anhydrate crystal energy landscape was calculated for Z′=1 and Z′=2 structures and complemented with the experimental structures (**Hy$_{dehy}$** – Z′=3 and **Form V** – Z′=4). The combined crystal energy landscape (Figure 11) has **Form V** as the lowest energy structure, albeit only by 0.32 kJ mol^{-1} with respect to the second lowest energy structure (**III**). **Forms III** (rank 2), **Hy$_{dehy}$** (rank 5) and **II** (rank 6) were all found among the lowest energy structures. With the exception of **Hy$_{dehy}$**, the six lowest energy packings show structural resemblance. One low density structure can be found in Figure 11, which corresponds to the isomorphic desolvate of the DDS dichloromethane hemisolate[40].

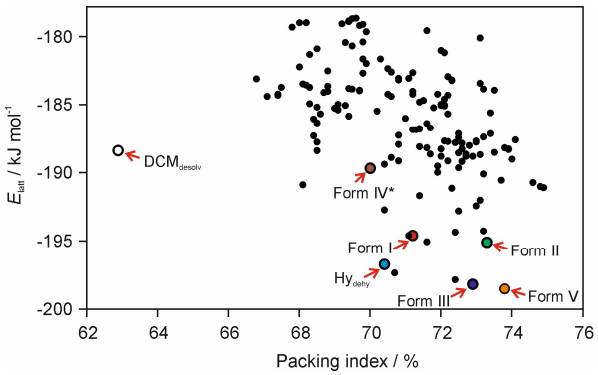

Figure 11. Summary of the crystal structure prediction for DDS (*Z′=1* & 2) complemented with experimental forms **Hy$_{dehy}$** (*Z′*=3) and **Form V** (*Z′*=4), with each symbol denoting a crystal structure by its lattice energy and packing index. Experimental forms are coded in color. Note that for **Form IV** only an ordered version can be found on the computed crystal energy landscape.

3.6.3. Forms I and IV

We were able to record the PXRD patterns for the two polymorphs, **Form I** and **IV**, which were obtained from the melt. Due to the sample preparation, from melt film preparations, and the fact that often the desired form had to be separated "*manually*" from **Form III** we could only gently grind the samples (to avoid transformation to **Form III** due to possible impurities) and therefore we did not attempt to solve the structures from powder data. Nevertheless, it was possible to index the PXRD patterns recorded for the two polymorphs. The cell parameters and experimental PXRD patterns were then compared to the lattice parameters of the predicted structures (Figure 11. Experimental and computed (simulated from the computed 0 K structures) PXRD patterns were also compared.

For **Form I,** the experimentally determined RT lattice parameters [*a*=19.3786(18) Å, *b*=8.3016(7) Å, *c*=16.4960(11) Å, *β*=114.533(3)°, Figure S1 of the Electronic Supporting Information] match the lattice parameters of the rank 8 structure (Figure 11), which was calculated to the 3.9 kJ mol^{-1} less stable than **Form V**. The rank 8 structure was then reoptimized using and fixing the lattice

parameters derived for **Form I**. The comparison of the experimental and simulated PXRD patterns shows an excellent agreement, confirming that the predicted rank 8 structure is indeed **Form I** (.res file for **Form I** is given in the Electronic Supporting Information). Furthermore, the computed energy differences [6.02 kJ mol^{-1} (PBE-TS) and 3.92 kJ mol^{-1} (PBE-D2, single point calculations using the PBE-TS structure)] are in reasonable agreement with the experimentally derived energy difference of 5.68 ± 0.27 kJ mol^{-1} between **Forms I** and **V**.

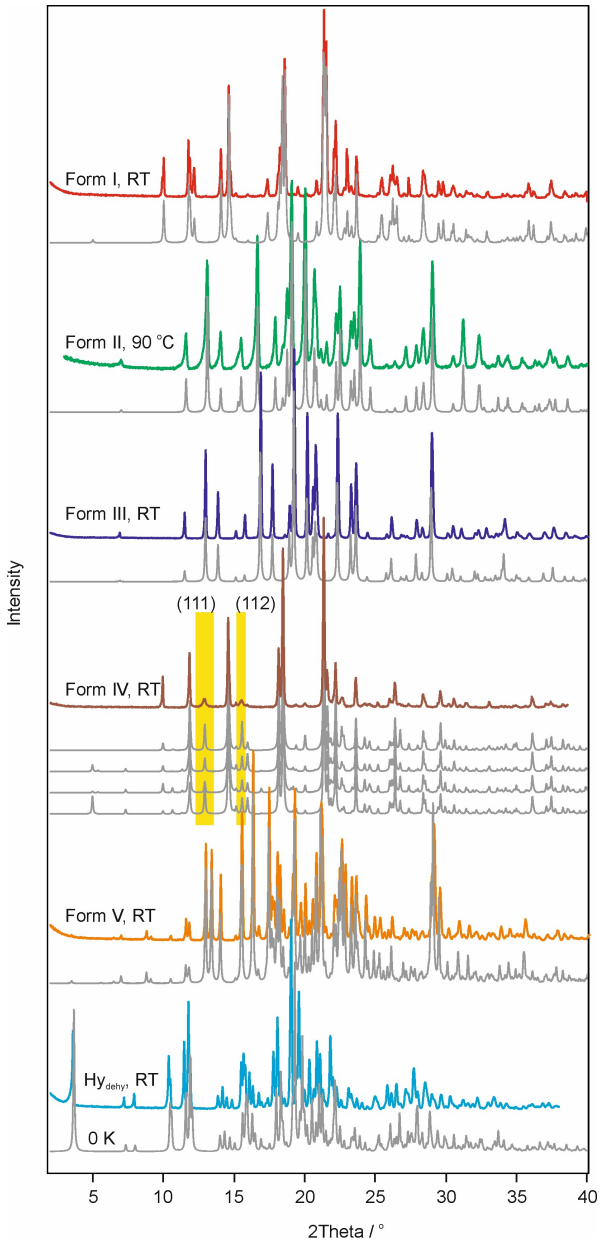

Figure 12. Experimental and computed PXRD diffractograms. The computed diffractograms for **Forms I – V** were generated by simulating the PXRD patterns from computed structures using fixed experimental lattice parameters and the predicted (**I – IV**) and experimental (**V**) structures as starting points. For **Form IV** different disorder models are given (with key areas highlighted) and for $\mathbf{Hy_{dehy}}$ the **0.33-Hy** structure was optimized without water (0 K structure).

The PXRD pattern of **Form IV** indexed to an orthorhombic cell [*a*= 16.4325 (8) Å, *b*= 8.3091(4) Å, *c*= 17.7345 (13), Z=8], however based on the data it was not possible to unambiguously derive the space group. A reasonable agreement between the experimental **Form IV** lattice parameters and experimental PXRD pattern was found with the rank 24 structure ($Pca2_1$, Z′=2, Z=8), a structure calculated to be 8.8 kJ mol^{-1} less stable than **Form V** (Figure S2 of the Electronic Supporting Information). A closer inspection of the experimental PXRD pattern revealed that certain reflections are broadened [in $Pca2_1$: (1 1 1) and (1 1 2)], indicating diffuse scattering/disorder. Interestingly, the rank 24 structure (transferred to P1) allowed the reorientation of dapsone molecules within the structure, a possibility for disorder. Optimization (lattice parameters and atomic positions) of the putative disordered structures resulted in lattice energy minima. More importantly, the structures did not distort during optimization and were in the lattice energy range of 13 kJ mol^{-1} with respect to **Form V**. The four computed PXRD patterns given in Figure 11 for **Form IV** correspond to the selection of structures given in Figure 13 (same order). A combination of the selected disorder models could account for the diffuse scattering observed for the **Form IV**, indicating that the rank 24 structure is an ordered version of the **Form IV**. The disorder in the experimental **Form IV** structure is expected to entropically favor the structure, thus lower the crystal energy.

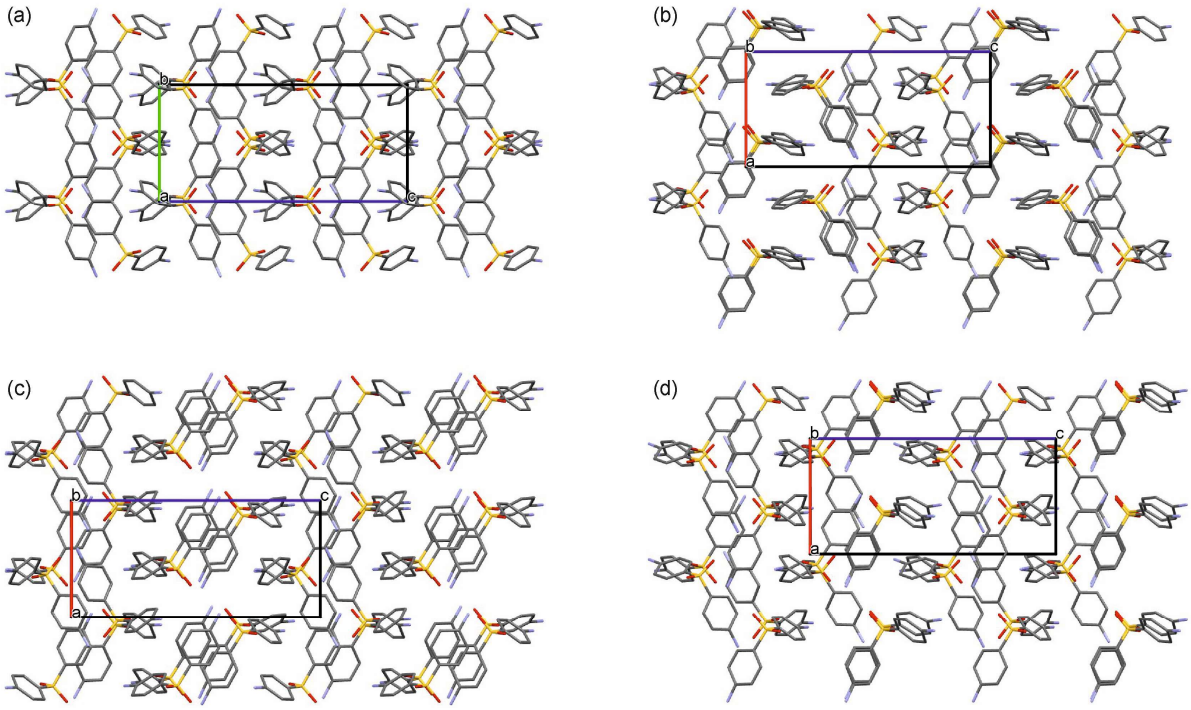

Figure 13. Comparison of (a) ordered (rank 24) structure of **Form IV** and (b-d) selected "disorder" models. Unit cells are shown.

The **Forms I** and **IV** show structural similarities but adopt distinct packing arrangements compared to the **Forms II**, **III** and **V** (Figure 9). Each of the two symmetry independent molecules of **Form I** forms two N–H···O hydrogen bonded chain motifs, leading to interpenetrating layers parallel to the *a* axis (Figure 14a). Furthermore, N–H···O interactions connect the layers. In addition to the hydrogen bonding interactions, π···π interactions, formed between inversion related DDS molecules, significantly contribute to the **Form I** lattice energy (see Section 8 of the Supporting Information).

Form IV* (ordered structure model) differs from **Form I** in that the layers are formed by symmetry independent molecules (Figure 14b) and that selected corresponding molecules in the two structures adopt mirror image positions, leading to different symmetry relations. The inversion related dimers of **Form I** can also be found in **Form IV***, albeit are formed between the

independent DDS molecules. The same type of strong N–H···O hydrogen bonding interactions, seen in **Form I**, are also formed in Form **IV***.

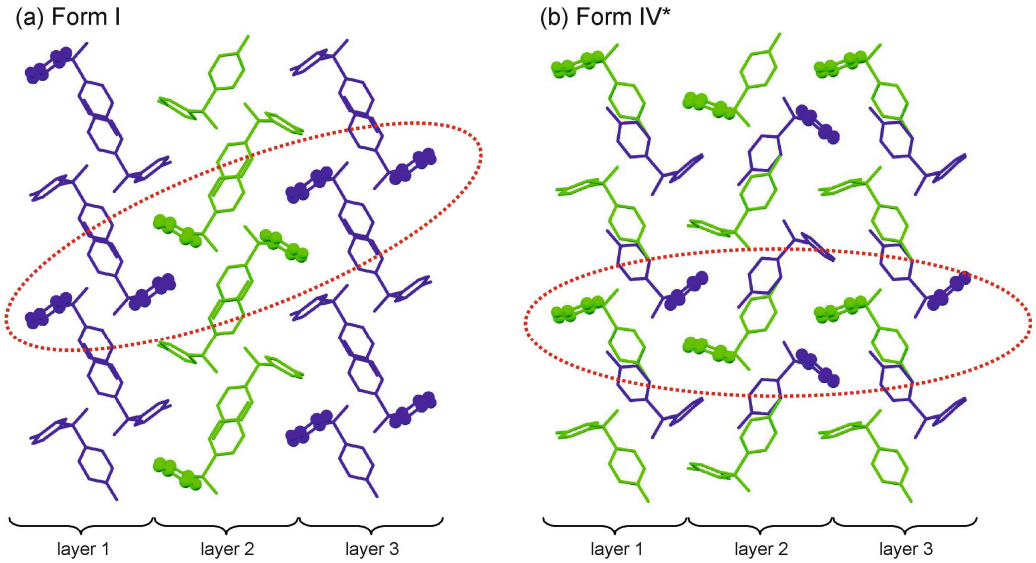

Figure 14. Packing comparison of (a) **Form I** and (b) **Form IV***. Symmetry equivalent molecules are depicted in the same color. Aminophenyl rings pointing out of the plane of projection are indicated with balls. Differences in packing are highlighted with a red dotted ellipsoid.

3.6.4. Isomorphic Dehydrate

As previously shown, it is possible to dehydrate the **0.33-Hy** to an isomorphic dehydrate structure.[42] The structure depicted in Figure 9f was obtained by computationally removing the water molecules in **0.33-Hy** and optimizing the structure. A structure comprising of the staring structure and the dehydrate structure confirmed isostructurality (Figure S13 of the Electronic Supplementary Information). The experimentally measured (< 1% RH) and simulated PXRD diffractograms, using the computed 0 K structure (Figure 12), are in excellent agreement. The packing observed for $\mathbf{Hy_{dey}}$ is distinct from all packings observed in the experimental (Figure 9) and computed Z′=1 & 2 DDS structures (Figure 11) and requires three symmetry independent molecules. The hydrate structure was successfully produced, but only form water. Crystallization

of DDS from organic solvents, which do not form a solvate with DDS, resulted invariably in **Form III** (or **II**).

4. Discussion

Dapsone shows a rich and diverse anhydrate solid form landscape (Figure 15), with intriguing solid form transformations and interesting structural features. The reinvestigation of the long-time known polymorphic system resulted in a novel anhydrate polymorph (**Form V**), which not only shows an unusually high Z′ number but is also more stable than all of the hitherto know solid forms of DDS at ambient conditions. The measured and calculated thermochemical data allowed us to assess the complex thermodynamic relationships of the polymorphs, visualized in a semi-schematic energy temperature diagram and confirming that the new **Form V** is indeed the stable polymorph in the temperature range from absolute zero to at least 90 °C. At higher temperatures **Form II** and then **Form I** are the polymorphs with the highest thermodynamic stability.

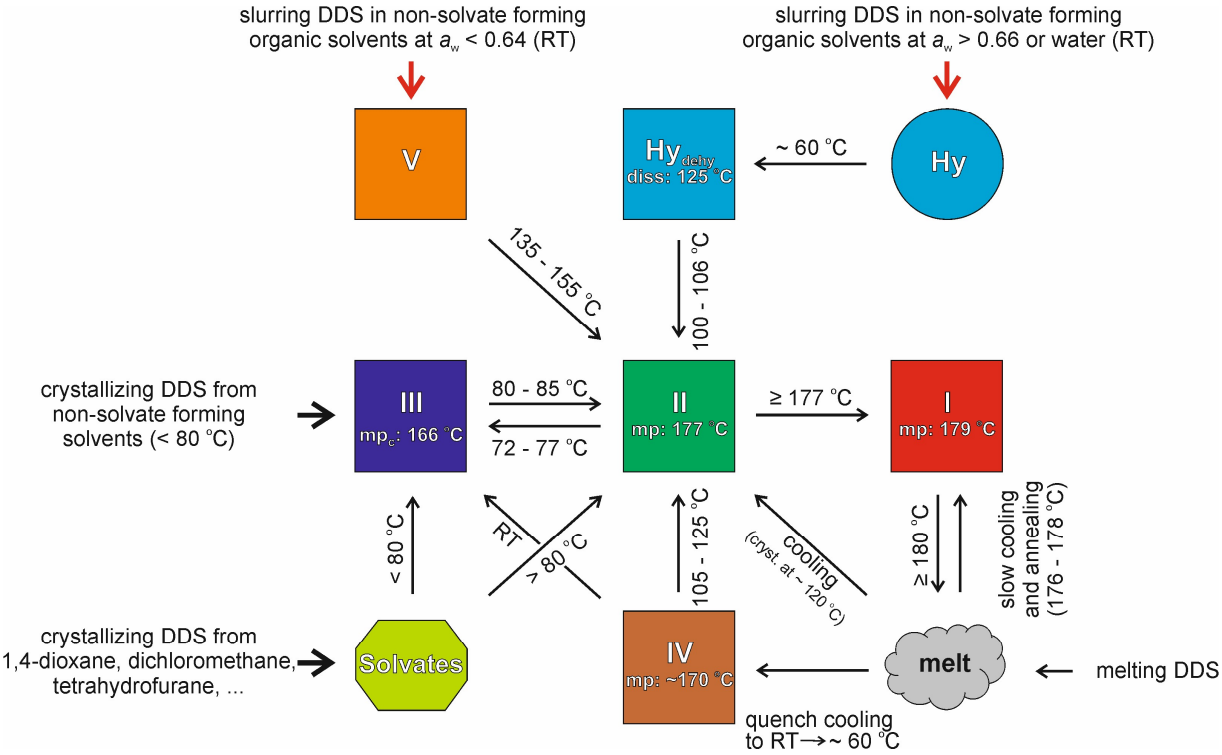

Figure 15. Preparation and transition pathways of the DDS solid forms at different temperatures. **I** – **V**: anhydrous forms; **Hy**: 0.33-hydrate; **Hy$_{dehy}$**: isostructural dehydrate; Solvates (dichloromethane, dioxane and tetrahydrofurane).

Despite being a small and "simple" molecule the substance represents a challenge to experimental and computational screening protocols. Computational screenings (CSP) for high Z′ structures are still problematic, even for small molecules like DDS, as the computational cost (time) increases exponentially for Z′ > 1 structures. Moreover, the fact that the thermodynamic room temperature form of this 100 years old compound stayed undiscovered to date, despite having been investigated by several groups, highlights that the experimental access to a stable form is not obvious and may require strategies, which are beyond routine solid form screening programs.

4.1. Why is Form V a Late-Appearing Form?

The easiest answer to the above question would be citing the famous statements in crystal polymorphism, which has stood the test of time: in 1965 Walter McCrone stated, "*It is at least this author's opinion that every compound has different polymorphic forms and that, in general, the number of forms known for each compound is proportional to the time and money spent in research on that compound*."[72] The statement in 1975, by Maria Kuhnert-Brandstaetter, "*Probably every substance is potentially polymorphous. The only question is, whether it is possible to adjust the external conditions in such a way that polymorphism can be realized or not*",[73] clearly reflects the challenges in solid form screening, that might be specific for the nucleation and growth of one solid-state form. Similarly to the recently reported case of the monohydrate polymorphs of 4-aminoquinaldine,[18] most solvent crystallization conditions result in **Form III**, which shows a very high kinetic stability and is thus readily observed. Even after a storage time of 40 years, mixtures of this form with the hydrate showed no transformation into the thermodynamically most stable **Form V**. The preferred occurrence of the metastable **Form III** is also the consequence of its fast nucleation and growth rate as evidenced from HSM and solvent crystallization experiments. However, at crystallization temperatures above 85 °C, the formation of **Form II** is favored in solvent crystallization experiments, which then readily transforms to the isosymmetric and enantiotropically related polymorph **Form III** upon cooling below 75 °C.

The recipe for preparing **Form V** is slurring DDS in a non-solvate forming solvent (or solvent mixture). The first slurry experiment that resulted in **Form V** used the **0.33-Hy** as starting phase but it was found that the procedure works also with any other DDS solid form as initial material. However, if the readily (and commercially) available **Form III** is used as a staring material the transformation is very slow. This observation appears surprising in view of the close structural resemblance between **Form III** and **Form V** (Figure 9). Nevertheless, the rearrangement (Figure

10) must have a high activation energy barrier, as manifested in the slow transformation kinetics in slurry experiments and the lack of transformation in the solid state.

One distinct and remarkable structural feature of **Form V** is the crystallization as a Z′=4 structure and another that one out of the four DDS molecules adopts a higher energy conformation, not seen in any of the other DDS structures. The fact that this Z′=4 structure is hard to produce, as opposed to the Z′=1 **Form III** structure, clearly contradicts the statement, "*a high Z' structure is a crystal on the way*."[74] The structural features of **Form V** are in agreement with the conclusion, that "*the molecular chemical nature of interactions drives crystal packing and not anthropomorphically imposed restraint of symmetry*",[75] as exemplified in the literature by the greater stability of symmetry-independent pairs in Z′=2 structures.[76, 77] The presence of an unusual conformation in the case of **Form V** can be justified by the gain in lattice energy stability, allowing more stable intermolecular interactions (closer contacts).

The late appearance of the thermodynamic form is consistent with Ostwald's rule of stages.[78, 79] To date, **Form V** has only been produced *via* transformation experiments. Seeding solvent crystallization experiments with **Form V** always resulted in **Form III** (provided a non-solvate forming solvent was used), possibly due to the structural resemblance of the fast nucleating and growing polymorph **III** and potentially the lack of the presence of the "distorted" high energy DDS conformation (Figure 8) in solution. Similarly, cooling a **Form V**-seeded DSS melt did not produce **Form V**. In contrast, by adjusting the crystallization temperatures/cooling rates it was possible to nucleate and grow the high temperature **Form I** or the metastable polymorph **Form IV**, in addition to **Forms II**/**III** from the melt. To conclude, the formation of the more complex packing of **Form V**, with its distinct conformation, requires more time than the crystallization of the structurally related Forms **II**/**III**. The **Forms II**/**III** as well as the hydrate do not undergo a

solid-solid transformation to **Form V** over decades at ambient storage conditions, indicating that the activation barrier of this reaction is high and that these phases are kinetically very stable. Therefore, the phase transformation to the stable room temperature **Form V** can only be triggered by sufficiently stressing the system, which can be successfully performed by slurry experiments.

4.2. Are there still undiscovered DDS Polymorphs?

Form V emerged as a "late appearing" stable form after decades considering **Form III** the thermodynamically stable form of DDS at room temperature.[25]. Hence, this reinvestigation highlights a serious problem in solid form screening, *i.e.* that finding the practically (most) useful solid form(s), including the most stable one, may not be a straight forward task. Due to the economic time pressure in the development of pharmaceutical products it is practically impossible to exploit all experimental conditions that may lead to different solid forms (e.g., [8-17]) and there is always the risk of missing relevant forms. The use of CSP as a complementary method to experimental screening can be highly advantageous in identifying putative other forms (e.g. creatine,[80] 4-aminoquinaldine,[18] carbamazepine,[9] dalcetrapib[81]). However, as demonstrated for DDS, CSP studies have limitations. Firstly, **Form II** might be missed due to the fact that in CSP protocols, the initially large number of generated structures are often rigorously minimized/clustered, resulting in identical **Form II/III** structures at 0 K (in agreement with the enantiotropic relationship of the two polymorphs!). Secondly, as seen in this work, limitations with respect to the number of symmetry independent molecules (only Z′=1 and 2) and conformations (using only the optimized conformation) had **Form III** as the most stable structure. **Form V** was not found in the computational screening, as a Z′=4 search was not attempted. The latter is also true for **Hy$_{dehy}$**, a Z′=3 structure. Unless a more exhaustive CSP would have been performed, the

computationally generated crystal energy landscape would not have hinted that a more stable polymorph is missing.

So far five polymorphs and the isostructural dehydrate have been confirmed experimentally for anhydrous DDS. An analysis of the low energy structures in Figure 11 reveals that there are other feasible sutures in the energy range expected for polymorphs. The lowest unobserved structures (rank 3, rank 4 & rank 7, see Electronic Supplementary Information) have packing features seen in Forms **III/II** and **V**. Interestingly, all of the hypothetical lowest energy structures generated in the search (5 kJ mol^{-1} range with respect to **Form V**) show a higher packing similarity with **Forms II**, **III** and **V**, than with Forms **I**, **IV** or **Hy$_{dehy}$** (Figure 16). The computational results indicate that other polymorph of DDS may exist. However, the isolation of a kinetically sufficiently stable Z′=1 or 2 structure from solution crystallization experiments requires the nucleation and growth of the Forms **II** and **III** to be impeded or prevented, as for example, is seen for 4-aminoquinaldine monohydrate where an impurity facilitates the growth of the stable polymorph.[18]

Overall, the packing comparisons of hypothetical and experimental structures reveal that interactions found in the experimental **Forms II**, **III** and **V** dominate the packing motifs seen in the most stable structures. Thus, from a statistical point of view it is more likely that a structure related to **II/III** nucleates (a big family of structure that have ≥ 8 molecules in common with **II/III**; Figure 16), which then may be able to template the growth of **Form II/III**, explaining why the latter forms are easily observed in solvent crystallization experiments. The three (from **Forms II/III** and **V**) most distinct low energy structures (Figure 11) are the hydrate (and **Hy$_{dehy}$**) and **Forms I** and **IV**, all experimentally found. The **Hy$_{dehy}$** needs the **0.33-Hy** as precursor and the two polymorphs can only be grown from the melt at specific temperatures/conditions.

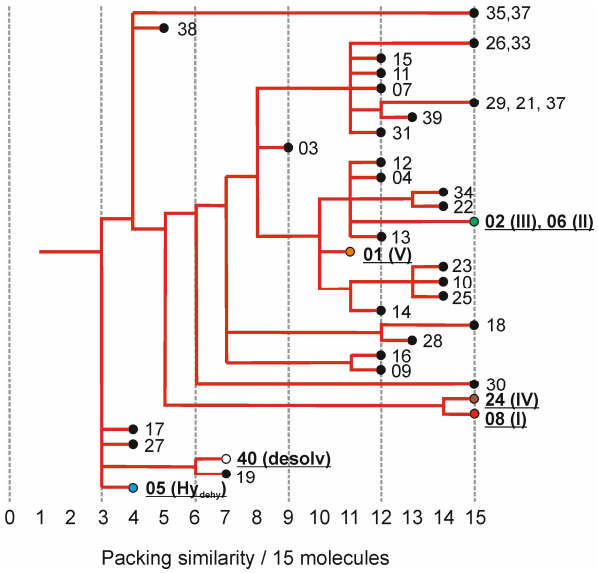

Figure 16. Dendrogram based on the experimental and lowest energy structures of DDS anhydrate solid forms linking structures based on their average packing similarity ($rmsd_{15}$; distance tolerance: 25%; angle tolerance: 25°).

5. Conclusions

The combination of computational chemistry, experimental screening and characterization allowed us to elucidate the structural, kinetic and thermodynamic stability interrelationships of the neat solid-state forms (**Forms I – V** and an **Hy$_{dehy}$**) of DDS. The finding of the thermodynamically most stable anhydrate at room temperature (**Form V**), eighty years after the therapeutic value of DDS has been recognized,[26, 27] was complicated by the fact that this high density form shows a slow nucleation and growth rate, in contrast to the metastable **Form III**. This metastable polymorph shows a remarkable kinetic stability, and is why no conversion to the thermodynamically stable **Form V** was observed during storage for forty years at ambient conditions. **Form V** was identified as the thermodynamically most stable polymorph in the temperature range from absolute zero to above 90 °C, above that temperature **Form II** becomes more stable and at highest temperatures **Form I**.

This study is another clear demonstration that by combining different experimental and computational approaches it is possible to derive many more structures of a highly polymorphic system, which then allows us to rationalize the overserved transformation and stability characteristics of the solid forms. Two of the structures were derived from CSP calculations (**I**, **IV**), **Hy**$_{\mathbf{dehy}}$ by computationally removing the water molecule from the hydrate, and **Form V** from PXRD supported with lattice energy calculations. The calculations confirmed the unusual features seen in **Form V**, *i.e.* $Z'=4$ and higher energy DDS molecular conformation. Furthermore, the lattice energy calculations correctly predicted the experimental 0 K stability order, affirming that the isomorphic dehydrate structure (**Hy**$_{\mathbf{dehy}}$) is within 2 kJ mol^{-1} in enthalpy of the most stable anhydrous form.

We have demonstrated that a deep understanding of crystal polymorphism in a complex system has been gained by combining the complementary information obtained from phenomenological, kinetic, thermodynamic, structural, and computational data. Moreover the extensive experimental work provides a plethora of data which can be used for improving and validating computational strategies for solid structure and energy prediction.

ASSOCIATED CONTENT

Supporting Information

The Supporting Information is available free of charge on the ACS Publications website at xxx.

Pawley fitting, Dapsone form **V**, computational generation of low-energy anhydrate structures, representation of the experimental structures, form **IV** modelling, CrystalExplorer calculations, *.res files (pdf)

Accession Codes

CCDC Accession Code 1911167 contains the supplementary crystallographic data for this paper, which can be obtained free of charge at www.ccdc.cam.ac.uk/data_request/cif, by emailing data_request@ccdc.cam.ac.uk, or contacting The Cambridge Crystallographic Data Centre, 12 Union Road, Cambridge CB2 1EZ, UK; fax: +44 1223 336033.

AUTHOR INFORMATION

Corresponding Author

* E-mail: doris.braun@uibk.ac.at

Author Contributions

The manuscript was written through contributions of all authors. All authors have given approval to the final version of the manuscript.

Funding Sources

FWF, project V436-N34

EU COST Action CM1402

Acknowledgment

The authors are grateful to Profs. C. C. Pantelides and C. S. Adjiman (Imperial College London) for the use of the CrystalPredictor and CrystalOptimizer programs and to Prof. S. L. Price (University College London) for the use of the DMACRYS program. Dr. Anthony Reilly is acknowledged for the packing similarity dendrogram script. DEB gratefully acknowledges funding by the Elise Richter programme of the Austrian Science Fund (FWF, project V436-N34).

The project benefited from EU COST Action CM1402 'Crystallize'. The computational results presented have been achieved using the HPC infrastructure LEO of the University of Innsbruck.

References

§ Crystal data of dapsone form **V**: $C_{12}H_{12}N_2O_2S$, M_r = 248.3, monoclinic, space group $P2_1/n$, Z′=4, T = 298 K, sample formulation: powder, wavelength: 1.54056 Å, a = 29.3396(3) Å, b = 5.84122(6) Å, c = 30.2717(3) Å , Volume = 4672.14(8) Å^3, Z = 14, density = 1.412 g cm^{-3}, 2 θ range for data collection: 2–70°, background treatment: Chebyshev polynomial, No. of measured reflections: 2060, Refinement method: rigid body Rietveld, Goodness of fit: 2.114 (on Y_{obs}), R_{wp} = 2.378, R_{exp} = 1.635, R_p = 1.871.

1. Aaltonen, J.; Alleso, M.; Mirza, S.; Koradia, V.; Gordon, K. C.; Rantanen, J. Solid form screening - A review. *Eur. J. Pharm. Biopharm* **2009,** *71*, (1), 23-37.
2. Singhal, D.; Curatolo, W. Drug polymorphism and dosage form design: a practical perspective. *Advanced Drug Delivery Reviews* **2004,** *56*, (3), 335-347.
3. Hilfiker, R.; Blatter, F.; von Raumer, M., Relevance of solid-state properties for pharmaceutical products. In *Polymorphism*, Hilfiker, R., Ed. 2006; pp 1-19.
4. Florence, A. J., Approaches to high-throughput physical form screening and discovery. In *Polymorphism of Pharmaceutical Solids* 2nd ed.; 2009; pp 139-184.
5. Boldyreva, E. V. High-pressure diffraction studies of molecular organic solids. A personal view. *Acta Crystallogr. , Sect. A: Found. Crystallogr* **2008,** *64*, (1), 218-231.
6. Moggach, S. A.; Parsons, S.; Wood, P. A. High-pressure polymorphism in amino acids. *Crystallogr. Rev* **2008,** *14*, (2), 143-184.
7. Fabbiani, F. P. A.; Allan, D. R.; David, W. I. F.; Davidson, A. J.; Lennie, A. R.; Parsons, S.; Pulham, C. R.; Warren, J. E. High-Pressure Studies of Pharmaceuticals: An Exploration of the Behavior of Piracetam. *Crystal Growth & Design* **2007,** *7*, (6), 1115-1124.

8. Zencirci, N.; Gelbrich, T.; Kahlenberg, V.; Griesser, U. J. Crystallization of Metastable Polymorphs of Phenobarbital by Isomorphic Seeding. *Cryst. Growth Des* **2009,** *9*, (8), 3444-3456.
9. Arlin, J. B.; Price, L. S.; Price, S. L.; Florence, A. J. A strategy for producing predicted polymorphs: catemeric carbamazepine form V. *Chemical Communications* **2011,** *47*, (25), 7074-7076.
10. Eccles, K. S.; Deasy, R. E.; Fabian, L.; Braun, D. E.; Maguire, A. R.; Lawrence, S. E. Expanding the crystal landscape of isonicotinamide: concomitant polymorphism and co-crystallisation. *CrystEngComm* **2011,** *13*, (23), 6923-6925.
11. Sridhar, B.; Nanubolu, J. B.; Ravikumar, K. The first polymorph in the family of nucleobases: a second form of cytosine. *Acta Crystallogr. , Sect. C: Struct. Chem* **2015,** *71*, (2), 128-135.
12. Pfund, L. Y.; Matzger, A. J. Towards Exhaustive and Automated High-Throughput Screening for Crystalline Polymorphs. *ACS Comb. Sci* **2014,** *16*, (7), 309-313.
13. Taleb, M.; Didierjean, C.; Jelsch, C.; Mangeot, J. P.; Capelle, B.; Aubry, A. Crystallization of proteins under an external electric field. *J. Cryst. Growth* **1999,** *200*, (3/4), 575-582.
14. Ruecroft, G.; Hipkiss, D.; Ly, T.; Maxted, N.; Cains, P. W. Sonocrystallization: The Use of Ultrasound for Improved Industrial Crystallization. *Org. Process Res. Dev* **2005,** *9*, (6), 923-932.
15. Sun, X. Y.; Garetz, B. A.; Myerson, A. S. Supersaturation and polarization dependence off polymorph control in the nonphotochemical laser-induced nucleation (NPLIN) of aqueous glycine solutions. *Crystal Growth & Design* **2006,** *6*, (3), 684-689.
16. Ikni, A.; Clair, B.; Scouflaire, P.; Veesler, S.; Gillet, J.-M.; El Hassan, N.; Dumas, F.; Spasojevic-de Bire, A. Experimental Demonstration of the Carbamazepine Crystallization from Non-photochemical Laser-Induced Nucleation in Acetonitrile and Methanol. *Cryst. Growth Des.* **2014,** *14*, (7), 3286-3299.
17. Lee, A. Y.; Lee, I. S.; Dettet, S. S.; Boerner, J.; Myerson, A. S. Crystallization on confined engineered surfaces: A method to control crystal size and generate different polymorphs. *Journal of the American Chemical Society* **2005,** *127*, (43), 14982-14983.

18. Braun, D. E.; Oberacher, H.; Arnhard, K.; Orlova, M.; Griesser, U. J. 4-Aminoquinaldine monohydrate polymorphism: prediction and impurity aided discovery of a difficult to access stable form. *CrystEngComm* **2016,** *18*, 4053-4067.
19. Price, S. L.; Reutzel-Edens, S. M. The potential of computed crystal energy landscapes to aid solid-form development. *Drug Discov Today* **2016,** *21*, (6), 912-923.
20. Chemburkar, S. R.; Bauer, J.; Deming, K.; Spiwek, H.; Patel, K.; Morris, J.; Henry, R.; Spanton, S.; Dziki, W.; Porter, W.; Quick, J.; Bauer, P.; Donaubauer, J.; Narayanan, B. A.; Soldani, M.; Riley, D.; McFarland, K. Dealing with the Impact of Ritonavir Polymorphs on the Late Stages of Bulk Drug Process Development. *Organic Process Research & Development* **2000,** *4*, (5), 413-417.
21. Perez-Lloret, S.; Rey, M. V.; Ratti, P. L.; Rascol, O. Rotigotine transdermal patch for the treatment of Parkinson's Disease. *Fundamental & Clinical Pharmacology* **2013,** *27*, (1), 81-95.
22. Price, S. L., Computational methodologies: towards crystal structure and polymorph prediction. In *Polymorphism in Pharmaceutical Solids*, 2 ed.; Brittain, H. G., Ed. Informa Healthcare USA, Inc.: New York, 2009; pp 53-76.
23. Price, S. L. Predicting crystal structures of organic compounds. *Chem Soc Rev* **2014,** *43*, 2098-2111.
24. Price, S. L.; Braun, D. E.; Reutzel-Edens, S. M. Can computed crystal energy landscapes help understand pharmaceutical solids? *Chem. Commun* **2016,** *52*, 7065-7077.
25. Fromm, E.; Wittmann, J. Derivatives of p-Nitrothiophenol. *Ber. Dtsch. Chem. Ges.* **1908,** *41*, 2264-73.
26. Wolf, R.; Orni-Wasserlauf, R. A century of the synthesis of dapsone: its anti-infective capacity now and then. *International journal of dermatology* **2000,** *39*, (10), 779-83.
27. Wozel, G.; Blasum, C. Dapsone in dermatology and beyond. *Archives of Dermatological Research* **2014,** *306*, (2), 103-124.
28. Organization, W. H. 20th WHO Model List of Essential Medicines. (http://www.who.int/medicines/publications/essentialmedicines/en/)
29. Kuhnert-Brandstatter, M.; Moser, I. Polymorphism of Dapson and ethambutoldihydrochloride. *Mikrochimica Acta* **1979,** *1*, (1-2), 125-136.

30. Brandstaetter-Kuhnert, M.; Kofler, A.; Hoffmann, R. Microscopic characterization and identification of pharmaceuticals. IV. *Sci. Pharm.* **1963,** *31*, (2), 140-8.
31. Braun, D. E.; Krueger, H.; Kahlenberg, V.; Griesser, U. J. Molecular Level Understanding of the Reversible Phase Transformation between Forms III and II of Dapsone. *Cryst. Growth Des.* **2017,** *17*, (10), 5054-5060.
32. Dickinson, C.; Stewart, J. M.; Ammon, H. L. X-ray crystal structure of the antimalarial and antileprotic drug, 4,4'-diaminodiphenyl sulfone. *J. Chem. Soc. D* **1970**, (15), 920-1.
33. Deo, N.; Tiwari, R. K.; Singh, T. P. Crystallization and x-ray crystal data of sulfonamides. *Journal of Scientific Research (Bhopal, India)* **1980,** *2*, (2), 137-9.
34. Bocelli, G.; Cantoni, A. Stereochemical studies of oligomers. XXVII. Reinvestigation of the structure of 4,4'-diaminodiphenyl sulfone. *Acta Crystallogr., Sect. C Cryst. Struct. Commun.* **1990,** *C46*, (11), 2257-9.
35. Su, G.; Pan, F.; He, Y.; Guo, S. Crystal structure and NLO properties of 4,4'-diaminodiphenylsulfone (DAPS). *Jiegou Huaxue* **1992,** *11*, (4), 293-6.
36. Bertolasi, V.; Ferretti, V.; Gilli, P.; De Benedetti, P. G. Molecular structure and crystal packing of five 4-aminophenyl (4-substituted phenyl) sulfones. Correlations between structural distortions, spectroscopic parameters and electronic substituent effects. *J. Chem. Soc., Perkin Trans. 2* **1993**, (2), 213-19.
37. Kuz'mina, L. G.; Struchkov, Y. T.; Novozhilova, N. V.; Tudorovskaya, G. L. Crystal structure of an aqueous solvate of p-diaminodiphenylsulfone. *Kristallografiya* **1981,** *26*, (4), 695-701.
38. Bel'skii, V. K.; Chernikova, N. Y.; Rotaru, V. K.; Kruchinin, M. M. Crystal and molecular structure of components of epoxy resins. II. 4,4'-Diaminodiphenyl sulfone hydrate. *Kristallografiya* **1983,** *28*, (4), 690-4.
39. H.S. Yathirajan, P. N., B. Nagaraj, B.L. Bhaskar, D.E. Lynch, 2004.
40. Lemmer, H.; Stieger, N.; Liebenberg, W.; Caira, M. R. Solvatomorphism of the Antibacterial Dapsone: X-ray Structures and Thermal Desolvation Kinetics. *Cryst. Growth Des.* **2012,** *12*, (3), 1683-1692.
41. Babashkina, M. G.; Safin, D. A.; Robeyns, K.; Brzuszkiewicz, A.; Kozlowski, H.; Garcia, Y. Thiophosphorylated bis-thioureas for competitive bulk liquid membrane transport of some metal ions. *CrystEngComm* **2012,** *14*, (4), 1324-1329.

42. Braun Doris, E.; Griesser Ulrich, J. Supramolecular Organization of Nonstoichiometric Drug Hydrates: Dapsone. *Frontiers in Chemistry* **2018,** *6*, Article 31.
43. Braun, D. E.; Gelbrich, T.; Kahlenberg, V.; Tessadri, R.; Wieser, J. a. G., Ulrich J. Conformational Polymorphism in Aripiprazole: Preparation, Stability and Structure of Five Modifications. *Journal of Pharmaceutical Sciences* **2009,** *98*, 2010-2026.
44. Braun, D. E.; McMahon, J. A.; Koztecki, L. H.; Price, S. L.; Reutzel-Edens, S. M. Contrasting Polymorphism of Related Small Molecule Drugs Correlated and Guided by the Computed Crystal Energy Landscape. *Cryst. Growth Des* **2014,** *14*, (4), 2056-2072.
45. Pawley, G. S. Unit-Cell Refinement from Powder Diffraction Scans. *Journal of Applied Crystallography* **1981,** *14*, (DEC), 357-361.
46. Coelho, A. A. *Topas Academic V5*, Coelho Software: Brisbane, 2012.
47. Frisch, M. J.; Trucks, G. W.; Schlegel, H. B.; Scuseria, G. E.; Robb, J. M. A.; Cheeseman, R.; Scalmani, G.; Barone, V.; Mennucci, B.; Petersson, G. A.; Nakatsuji, H.; Caricato, M.; Li, X.; Hratchian, H. P.; Izmaylov, A. F.; Bloino, J.; Zheng, G.; Sonnenberg, J. L.; Hada, M.; Ehara, M.; Toyota, K.; Fukuda, R.; Hasegawa, J.; Ishida, M.; Nakajima, T.; Honda, Y.; Kitao, O.; Nakai, H.; Vreven, T.; Montgomery, J. A.; Peralta, J. E.; Ogliaro, F.; Bearpark, M.; Heyd, J. J.; Brothers, E.; Kudin, K. N.; Staroverov, V. N.; Kobayashi, R.; Normand, J.; Raghavachari, K.; Rendell, A.; Burant, J. C.; Iyengar, S. S.; Tomasi, J.; Cossi, M.; Rega, N.; Millam, J. M.; Klene, M.; Knox, J. E.; Cross, J. B.; Bakken, V.; Adamo, C.; Jaramillo, J.; Gomperts, R.; Stratmann, R. E.; Yazyev, O.; Austin, A. J.; Cammi, R.; Pomelli, C.; Ochterski, J. W.; Martin, R. L.; Morokuma, K.; Zakrzewski, V. G.; Voth, G. A.; Salvador, P.; Dannenberg, J. J.; Dapprich, S.; Daniels, A. D.; Farkas; Foresman, J. B.; Ortiz, J. V.; Cioslowski, J.; Fox, D. J. *Gaussian 09*, Gaussian Inc.: Wallingford CT, 2009.
48. M. J. Turner, J. J. M., S. K. Wolff, D. J. Grimwood, P. R. Spackman, D. Jayatilaka, M. A. Spackman *CrystalExplorer17*, University of Western Australia, http://hirshfeldsurface.net., 2017.
49. Karamertzanis, P. G.; Pantelides, C. C. Ab initio crystal structure prediction - I. Rigid molecules. *Journal of Computational Chemistry* **2005,** *26*, (3), 304-324.
50. Karamertzanis, P. G.; Pantelides, C. C. Ab initio crystal structure prediction. II. Flexible molecules. *Molecular Physics* **2007,** *105*, (2-3), 273-291.

51. Habgood, M.; Sugden, I. J.; Kazantsev, A. V.; Adjiman, C. S.; Pantelides, C. C. Efficient Handling of Molecular Flexibility in Ab Initio Generation of Crystal Structures. *J. Chem. Theory Comput* **2015,** *11*, (4), 1957-1969.
52. Coombes, D. S.; Price, S. L.; Willock, D. J.; Leslie, M. Role of Electrostatic Interactions in Determining the Crystal Structures of Polar Organic Molecules. A Distributed Multipole Study. *Journal of Physical Chemistry* **1996,** *100*, (18), 7352-7360.
53. Breneman, C. M.; Wiberg, K. B. Determining Atom-Centered Monopoles From Molecular Electrostatic Potentials - The Need For High Sampling Density in Formamide Conformational-Analysis. *Journal of Computational Chemistry* **1990,** *11*, (3), 361-373.
54. Price, S. L.; Leslie, M.; Welch, G. W. A.; Habgood, M.; Price, L. S.; Karamertzanis, P. G.; Day, G. M. Modelling organic crystal structures using distributed multipole and polarizability-based model intermolecular potentials. *Phys. Chem. Chem. Phys.* **2010,** *12*, (30), 8478-8490.
55. Stone, A. J. Distributed multipole analysis: Stability for large basis sets. *Journal of Chemical Theory and Computation* **2005,** *1*, (6), 1128-1132.
56. Stone, A. J. *GDMA: A Program for Performing Distributed Multipole Analysis of Wave Functions Calculated Using the Gaussian Program System*, 2.2; University of Cambridge: Cambridge, United Kingdom, 2010.
57. Kazantsev, A. V.; Karamertzanis, P. G.; Adjiman, C. S.; Pantelides, C. C. Efficient Handling of Molecular Flexibility in Lattice Energy Minimization of Organic Crystals. *J. Chem. Theory Comput* **2011,** *7*, (6), 1998-2016.
58. Clark, S. J.; Segall, M. D.; Pickard, C. J.; Hasnip, P. J.; Probert, M. J.; Refson, K.; Payne, M. C. First principles methods using CASTEP. *Zeitschrift fur Kristallographie* **2005,** *220*, (5-6), 567-570.
59. Perdew, J. P.; Burke, K.; Ernzerhof, M. Generalized gradient approximation made simple. *Physical Review Letters* **1996,** *77*, (18), 3865-3868.
60. Vanderbilt, D. Soft Self-Consistent Pseudopotentials in a Generalized Eigenvalue Formalism. *Physical Review B* **1990,** *41*, (11), 7892-7895.
61. Tkatchenko, A.; Scheffler, M. Accurate Molecular Van Der Waals Interactions from Ground-State Electron Density and Free-Atom Reference Data. *Phys. Rev. Lett* **2009,** *102*, (7), 073005/1-073005/4.

62. Grimme, S. Semiempirical GGA-type density functional constructed with a long-range dispersion correction. *J. Comput. Chem* **2006,** *27*, (15), 1787-1799.
63. Burger, A.; Ramberger, R. On the polymorphism of pharmaceuticals and other molecular crystals. I. Theory of thermodynamic rules. *Mikrochimica Acta* **1979,** *2*, (3-4), 259-271.
64. Burger, A.; Ramberger, R. On the polymorphism of pharmaceuticals and other molecular crystals. II. Applicability of thermodynamic rules. *Mikrochimica Acta* **1979,** *2*, (3-4), 273-316.
65. Martins, M. H.; Calderini, A.; Pessine, F. B. T. Host-guest interactions between dapsone and β-cyclodextrin (Part II): thermal analysis, spectroscopic characterization, and solubility studies. *J. Inclusion Phenom. Macrocyclic Chem.* **2012,** *74*, (1-4), 109-116.
66. Linderstroem-Lang, C. U.; Naylor, R. F. 4,4'-Diaminodiphenyl sulfone: solubility and distribution in blood. *Biochemical Journal* **1962,** *83*, 417-20.
67. Reutzel-Edens Susan, M.; Braun Doris, E.; Newman Ann, W., Hygroscopicity and Hydrates in Pharmaceutical Solids. In *Polymorphism in the Pharmaceutical Industry: Solid Form and Drug Development*, Hilfiker, R.; Von Raumer, M., Eds. Wiley-VCH: 2018; Vol. 2nd.
68. Grunenberg, A.; Henck, J. O.; Siesler, H. W. Theoretical derivation and practical application of energy/temperature diagrams as an instrument in preformulation studies of polymorphic drug substances. *International Journal of Pharmaceutics* **1996,** *129*, (1,2), 147-158.
69. Yu, L. Inferring Thermodynamic Stability Relationship of Polymorphs from Melting Data. *Journal of Pharmaceutical Sciences* **1995,** *84*, (8), 966-974.
70. Griesser, U. J.; Weigand, D.; Rollinger, J. M.; Haddow, M.; Gstrein, E. The Crystal Polymorphs of Metazachlor: Identification and thermodynamic stability. *Journal of Thermal Analysis and Calorimetry* **2004,** *77*, 511-522.
71. Braun, D. E.; Gelbrich, T.; Kahlenberg, V.; Tessadri, R.; Wieser, J.; Griesser, U. J. Conformational Polymorphism in Aripiprazole: Preparation, Stability and Structure of Five Modifications. *Journal of Pharmaceutical Sciences* **2009,** *98*, (6), 2010-2026.
72. McCrone, W. C. Polymorphism. *Physics and Chemistry of the Organic Solid State* **1965**, (2), 725-767.
73. Kuhnert-Brandstaetter, M. A. *Pharm. Unserer Zeit* **1975**, 131-137.
74. Desiraju, G. R. On the presence of multiple molecules in the crystal asymmetric unit (Z ' > 1). *CrystEngComm* **2007,** *9*, (1), 91-92.

75. Steed, K. M.; Steed, J. W. Packing Problems: High Z' Crystal Structures and Their Relationship to Cocrystals, Inclusion Compounds, and Polymorphism. *Chemical Reviews (Washington, DC, United States)* **2015,** *115*, (8), 2895-2933.
76. Pidcock, E. Spatial arrangement of molecules in homomolecular Z' = 2 structures. *Acta Crystallogr., Sect. B Struct. Sci.* **2006,** *B62*, (2), 268-279.
77. Gavezzotti, A. Structure and energy in organic crystals with two molecules in the asymmetric unit: causality or chance? *CrystEngComm* **2008,** *10*, (4), 389-398.
78. Threlfall, T. Structural and thermodynamic explanations of Ostwald's rule. *Organic Process Research & Development* **2003,** *7*, (6), 1017-1027.
79. Ostwald, W. The formation and changes of solids. *Zeitschrift fuer Physikalische Chemie, Stoechiometrie und Verwandtschaftslehre* **1897,** *22*, 289-330.
80. Braun, D. E.; Orlova, M.; Griesser, U. J. Creatine: Polymorphs Predicted and Found. *Cryst. Growth Des* **2014,** *14*, (10), 4895-4900.
81. Neumann, M. A.; van de Streek, J.; Fabbiani, F. P. A.; Hidber, P.; Grassmann, O. Combined crystal structure prediction and high-pressure crystallization in rational pharmaceutical polymorph screening. *Nat. Commun* **2015,** *6*, 7793.

For Table of Contents Only